Desalination 507 (2021) 115032

Contents lists available at ScienceDirect

Desalination

journal homepage: www.elsevier.com/locate/desal

# Integrated novel solar distillation and solar single-effect absorption systems

Ahmad K. Sleiti *, Wahib A. Al-Ammari, Mohammed Al-Khawaja

*Department of Mechanical & Industrial Engineering, College of Engineering, Qatar University, Qatar*

## HIGHLIGHTS

- Novel hybrid solar distillation system integrated with solar absorption cooling
- Cost effective production of cooling and freshwater, simultaneously
- Novel and strategic integration of the two systems with no significant penalties
- Still productivity is three times higher and absorption system COP is 26% higher.
- Multi-objective optimization and analysis of the integrated system

## ARTICLE INFO

*Keywords:*
Absorption
Solar still
Distillation
Cooling
Lithium bromide
COP

## ABSTRACT

Novel hybrid single-slope solar distillation systems integrated with single-effect solar absorption cooling system are designed, analyzed and optimized for production of cooling effect and freshwater, simultaneously. The innovative integrated systems are capable of recovering significant portion of the released heat of their own components that is otherwise wasted; with superior performance and lower cost than available systems. The integration of the two solar systems is proposed in three strategic heat recovery configurations: (S1) recovers waste heat from the water vapor leaving the generator, (S2) recovers waste heat from the strong lithium bromide solution leaving the generator, and (S3) recovers waste heat from the hot liquid water leaving the generator. The results show that the productivity of the still is boosted by three-folds compared to the conventional system. S2 negatively affects the COP of the absorption system, however, it improves still productivity to higher values than S1.The COP of S3 is comparable to S1, while the still productivity of S3 is the highest with only slight increase in the area of the evacuated tube collector. S1 has the advantage of enhancing the still productivity and reducing the condenser cooling load without affecting the COP of the basic absorption system. The integrated system achieved an impressive cooling capacity of 20 kW, and still productivity of 10 kg/m$^2$-day with COP of 0.85 at conservative solar radiation of 500 W/m$^2$. The cost of the distilled water in S3 (0.047 $/kg) is lower than in S2 (0.054 $/kg) and S1 (0.061 $/kg).

## 1. Introduction

Development of technologies for superior refrigeration, air conditioning, and fresh water production is one of the top priorities, especially in hot and dry climate regions. Heating Ventilation and Air Conditioning (HVAC) systems consume large amount of energy; in the Gulf countries, for example, HVAC systems consume >67% of the total energy consumption [1]. The economic and environmental costs of producing these fundamental human needs using conventional methods (fossil fuel-powered systems) are too high with depressing effects on global warming and ozone depletion [2]. Furthermore, fossil fuels are not sustainable and might be depleted in the future, which makes the transition to sustainable resources unavoidable [3,4]. This strongly emphasizes the need to develop sustainable systems that provide power, cooling, heating, and fresh water at low cost and environmental penalties. The availability of solar energy in abundance in some regions of the world (especially in the Gulf region) increases the attractiveness of the solar thermal systems over those run by wind, biomass, or geothermal sources. Those systems will be even more attractive when combining them to produce both cooling/refrigeration and fresh water. Hence, in this paper, a novel hybrid solar absorption cooling system integrated with solar distillation system is introduced, analyzed and optimized for best performance and cost. The novelty aspects of the

* Corresponding author.
*E-mail address:* asleiti@qu.edu.qa (A.K. Sleiti).

https://doi.org/10.1016/j.desal.2021.115032
Received 19 November 2020; Received in revised form 19 February 2021; Accepted 23 February 2021
Available online 10 March 2021

**Nomenclature**

| | |
|---|---|
| $A_{ETC}$ | area of the evacuated tube collectors, $m^2$ |
| $A_{gl}$ | area of the glass cover of the still, $m^2$ |
| $A_{hc}$ | surface area of the heating coil, $m^2$ |
| $A_{sw}$ | area of the saline water in the basin of the still, $m^2$ |
| $C$ | constant in Dunkle's model, Eq. (32) |
| $C_{min}$ | minimum heat capacity rate, W/°C |
| $C_{ss}$ | heat capacity rate of the strong solution, W/°C |
| $C_{ws}$ | heat capacity rate of the weak solution, W/°C |
| $c_{p,\ ss}$ | specific heat of the strong solution, J/kg-°C |
| $c_{p,\ ws}$ | specific heat of the weak solution, J/kg-°C |
| $c_{p,\ r}$ | specific heat of the refrigerant vapor (water), J/kg-°C |
| $c_{p,\ v}$ | specific heat of the distilled water vapor, J/kg-°C |
| $c_{p,\ 10}$, $c_{p,\ 14}$ | specific heat at state points in Figs. 1 to 5, J/kg-°C |
| $D_{hc}$ | diameter of the heating coil, m |
| $F_R$ | heat removal factor of the evacuated tube collectors |
| $G$ | solar radiation intensity, $W/m^2$ |
| $Gr$ | Grashof number, |
| $g$ | gravitational acceleration, $m/s^2$ |
| $h_1$, $h_2$, … | specific enthalpies at state points in Figs. 1 to 5, J/kg |
| $h_{c,\ gl-a}$ | convective heat transfer coefficient between the glass cover and ambient air, $W/m^2$-°C |
| $h_{c,\ sw-gl}$ | convective heat transfer coefficient between the saline water and the glass cover, $W/m^2$-°C |
| $h_{ev,\ sw-gl}$ | evaporative heat transfer coefficient between the saline water and the glass cover, $W/m^2$-°C |
| $h_{fg}$ | enthalpy of vaporization, J/kg |
| $h_{hc,\ i}$ | heat transfer coefficient inside the heating coil, $W/m^2$-°C |
| $h_{hc,\ o}$ | heat transfer coefficient outside the heating coil, $W/m^2$-°C |
| $k_{hc}$ | thermal conductivity of the heating coil fluid, W/m-°C |
| $k_v$ | thermal conductivity of the distilled water vapor, W/m-°C |
| $L_{hc}$ | length of the heating coil, m |
| $L_v$ | average distance between the saline water and the glass cover, m |
| $m_{distilled}$ | mass of the distilled water, kg |
| $\dot{m}_1, \dot{m}_2, \ldots$ | mass flow rates at state points in Figs. 1 to 5, kg/s |
| $\dot{m}_{hc}$ | mass flow rate of the heating coil fluid, kg/s |
| $\dot{m}_r$ | mass flow rate of the refrigerant (water), kg/s |
| $Nu_{hc}$ | Nusselt number of the heating coil fluid, |
| $n$ | constant in Dunkle's model, Eq. (32), |
| $P_2$, $P_3$, … | pressure at state points in Figs. 1 to 5, Pa |
| $P_e$ | evaporator pressure, Pa |
| $P_{gl}$ | effective vapor pressure at the cover glass surface, Pa |
| $P_{sw}$ | effective vapor pressure at the saline water surface, Pa |
| $Pr_{hc,\ i}$ | Prandtl number of the heating coil fluid |
| $Q_a$ | heat released by the absorber, W |
| $Q_c$ | heat rejected by the condenser, W |
| $Q_{cc}$ | heat absorbed by the cooling coil, W |
| $Q_{c,\ sw-gl}$ | heat transferred by convection between the saline water and the glass cover, W |
| $Q_{c,\ gl-a}$ | heat transferred by convection between the glass cover and ambient air, W |
| $Q_{ETC}$ | heat incident on the evacuated tube collector by the sun, W |
| $Q_e$ | cooling capacity of the evaporator, W |
| $Q_{ev,\ sw-gl}$ | evaporative heat of the saline water, W |
| $Q_g$ | heat absorbed by the generator, W |
| $Q_{hc}$ | heat transferred to the saline water by the heating coil, W |
| $Q_r$ | heat recovered by the regenerator (solution heat exchanger), W |
| $Q_{r,\ sw-gl}$ | heat transferred by radiation between the saline water and the glass cover, W |
| $Q_{r,\ gl-sky}$ | heat transferred by radiation between the glass cover and sky, W |
| $Q_{sun}$ | heat incident on the saline water by the sun, W |
| $Re_{hc}$ | Reynolds' number of the heating coil fluid, |
| $T_1$, $T_2$, … | temperatures at state points in Figs. 1 to 5, °C |
| $T_a$ | ambient air temperature, °C |
| $T_{avg,\ hc}$ | average temperature of the heating coil fluid, °C |
| $T_{coll,\ in}$ | inlet temperature of water into the evacuated tube collectors, °C |
| $T_{gl}$ | glass cover temperature, °C |
| $T_{in,\ hc}$ | inlet temperature of the heating coil fluid, °C |
| $T_{out,\ hc}$ | outlet temperature of the heating coil fluid, °C |
| $T_{sky}$ | effective temperature of the sky, °C |
| $T_{sw}$ | temperature of the saline water, °C |
| $U_{hc}$ | overall heat transfer coefficient of the heating coil, $W/m^2$-°C |
| $U_L$ | overall hat transfer coefficient of the heat losses from the evacuated tube collectors, $W/m^2$-°C |
| $v_3$ | specific volume of the weak solution at the inlet of pump 1, $m^3/kg$ |
| $V_{wind}$ | wind speed, m/s |
| $W_{p1}$ | power consumed by pump 1, W |
| $x_1$, $x_2$, … | concentrations of the water/lithium bromide solution at state points in Figs. 1 to 5, % |

*Greeks symbols*

| | |
|---|---|
| $\alpha_{ETC}$ | absorptivity of the evacuated tube collectors |
| $\alpha_w$ | absorptivity of the saline water |
| $\varepsilon_{g-sky}$ | emissivity between the glass cover and sky |
| $\varepsilon_{sw-gl}$ | emissivity between the saline water and the glass cover |
| $\varepsilon_{SHX}$ | effectiveness of the solution heat exchanger |
| $\mu_{hc}$ | viscosity of the heating coil fluid, kg/m-s |
| $\mu_v$ | viscosity of the distilled water vapor, kg/m-s |
| $\eta_{ETC}$ | efficiency of the evacuated tube collectors, % |
| $\eta_{p1}$ | isentropic efficiency of pump 1 |
| $\eta_{ss}$ | efficiency of the solar still |
| $\sigma$ | Stefan-Boltzmann constant, $\sigma = 5.67 \times 10^{-8} \frac{W}{m^2K^4}$ |
| $\rho_v$ | density of the distilled water vapor, $kg/m^3$ |
| $\tau_{gl}$ | transmissivity of the glass cover |
| $\tau_{ETC}$ | transmissivity of the evacuated tube collectors |

*Abbreviations*

| | |
|---|---|
| COP | coefficient of performance |
| CSS | classical solar still |
| ECP | energy conservation principle |
| ETCs | evacuated tube collectors |
| EV1, EV2 | expansion valve 1, expansion valve 2 |
| EP | energy performance |
| HTF | heat transfer fluid |
| HVAC | Heating Ventilation and Air Conditioning |
| ORC | organic Rankine cycle |
| S1 | configuration 1, Fig. 3 |
| S2 | configuration 2, Fig. 4 |
| S3 | configuration 3, Fig. 5 |
| PBP | payback period |

combined system and the choice of the solar absorption system over other thermal refrigeration systems are discussed next.

Thermal refrigeration systems are categorized into two groups: thermo-mechanical systems and sorption systems (in open or closed forms). Sleiti et al. [5] conducted a detailed review of the innovative approaches of the thermo-mechanical refrigeration (TMR) systems including ejector systems, organic Rankine cycle (ORC) systems, and other isobaric/isothermal refrigeration systems [6,7]. They concluded that the major challenges of the ejector cooling system are the unavoidable ejector performance degradation at off-design conditions. The ORC is a proven and mature technology, however, it is more expensive than other systems and does not operate efficiently at temperatures lower than 100 °C. In contrast, the absorption systems are not sensitive to the variation of the operating conditions and able to effectively operate at temperatures lower than 100 °C [8]. In addition, sorption systems are more attractive when sources of low-grade thermal energy are available free or at low cost (such as solar energy or waste heat).

Absorption refrigeration is one of the most common sorption technologies [9] that started to gain noticeable share in refrigeration market. Furthermore, it consumes very low electric input (in continuous operation systems) or no electric input (in intermittent operation systems) [10]. Compared to the adsorption systems, the absorption systems are more compact for the same capacity due to the low specific cooling power of the adsorbent. Thermodynamically, there are three types of the absorption systems: single-effect, double-effect, and triple-effect absorption systems [8,9,11–14]. In general, the typical coefficient of performance (COP) of the triple effect (COP = 1.7) is higher than the double effect (COP = 1.2) and single effect (COP = 0.7) [15]. While the COP of the single effect system is the lowest, it works at lower temperatures and less expensive than double or triple systems [16]. The various techniques of improving absorption cooling systems are reviewed by Nikbakhti et al. [17] including the development of new operating fluids pairs, adding auxiliary components, and improving the operating conditions, They concluded that attempts made to improve the performance of the single effect system resulted in increasing its cost or/and complexity. As a result, the standard single-effect absorption system is considered suitable option for domestic refrigeration and air conditioning systems (especially in remote rural countries). It is worth mentioning that single-effect absorption systems working with water/lithium bromide pair are more advantageous for air conditioning applications than ammonia/water pair. The latter is toxic, has dangerous effect on health and it works at higher pressure. However, lithium bromide is relatively expensive.

The shortage of drinking water is a crucial issue in hot and dry climate regions, so efficient and durable water production systems need to be developed. The single-slope solar distillation unit is considered the simplest and the lowest cost system to distil brackish water. Researchers' efforts towards improving this basic system can be classified into three directions. The first direction is the introduction of new geometries rather than single-slope such as double-slope [18,19], tubular [20–22], spherical [23], pyramid [24,25], and stepped-basin solar stills [26]. The second direction is the integration of the solar still unit with flat plate/parabolic solar collectors [27,28], tubular solar-energy collector [29,30] or solar dish concentrators [31]. The third direction is the enhancement of solar still productivity via different means; such as using phase change materials [32–35], using nanofluids [36–40], using wire mesh packing [41], cooling of the glass cover [42], cooling of the water vapor by thermoelectric cooler [43–46], or by enhancing the evaporation process by the integration with the photovoltaic (PV) cells [47]. To avoid the complexity of the solar distillation unit and to maintain its simplicity and low cost, and to achieve higher production, the integration of the solar still with other efficient and low-cost thermal systems is recommended.

Sleiti et al. [48] investigated a novel solar ejector cooling system integrated with solar still. They found that the productivity of the still increases five times higher than the conventional one by enhancing water vaporization and condensation. Also, the integration of these systems slightly increases the required solar collector area without remarkable reduction of the COP of the system. However, as mentioned above, the ejector operation is sensitive to the operating conditions and it needs complex mechanisms to maintain stable operation. In contrast, the absorption system is stable with the variation of the operating conditions and at partial cooling loads.

Based on the above, a novel design of single-effect absorption system integrated with a solar distillation system is proposed, investigated and optimized in the present study. The novelty aspects of the proposed system include: (i) novel design of solar still system integrated with solar absorption system not studied before, (ii) recovering significant portion of the released heat of the components of the system that is otherwise wasted and (iii) optimizing the integrated system for superior performance and lower cost than existing (not integrated) systems. Three novel configurations are investigated to recover waste heat from the absorption system. Configuration 1 utilizes the solar still strategically before the condenser of the absorption system to enhance the productivity of the still and to reduce the cooling load of the condenser. The second configuration investigates the use of the solar still before the sensible heat exchanger (SHX) and the third configuration utilizes the solar still before the evacuated tube collectors to recover the excess energy of the heat transfer fluid after leaving the generator. These design configurations are explained in detail in Section 2. The developed thermodynamic models coupled with accurate models for the heat transfer coefficient inside the heating coil of the proposed design configurations are presented in Section 3 along with their validation. The sensitivity of the proposed system to the operating parameters, ambient conditions, and the cost estimation of the distilled water is discussed in Section 4.

## 2. System description

### 2.1. Components and operating mechanisms of the basic systems

Before the discussion of the proposed integration between the solar absorption and distillation systems, the basic configurations and operating mechanisms of the solar absorption system and the solar still system are described. As presented in Fig. 1, the basic single-stage cooling absorption system is similar to the basic vapor-compression cooling system with replacing the mechanical compressor by a thermal compression process. The thermal compressor consists of an absorber, pump, generator, and solution heat exchanger (SHX). It performs the compression process of the refrigerant using thermal energy as input with small mechanical energy to drive the liquid pump. The fundamental concept of the absorption cooling system is to pump the refrigerant in the liquid phase instead of the vapor phase, which greatly minimizes the required energy to produce cooling. The phase change of the refrigerant from the vapor to the liquid is performed in the absorber. As shown in Fig. 1, the refrigerant vapor enters the absorber at low temperature and pressure (state 2). Then, the refrigerant is absorbed by the strong solution (state 8) and the heat of absorption ($Q_a$) is released to an external heat sink (cooling water). The weak solution (state 3) is pumped to the generator pressure by pump 1. The pressurized solution flows through the SHX and heated up before entering the generator (states 4–5). In the generator, the weak solution is heated by an external heat source (solar energy in the present study) to vaporize the refrigerant (state 9), while the produced hot strong solution flows back through the SHX (states 6–7), and throttled by the expansion valve to the absorber (state 8). The high-pressure refrigerant vapor enters the condenser (state 10) and leaves the condenser as a high-pressure liquid (state 11). This high-pressure refrigerant liquid is throttled in the expansion valve ($EV_2$) to the evaporator (state 12) to absorb heat from the chilled water and leaves the evaporator as a vapor (state 1), completing the cycle. The SHX is used in the system to improve the COP by reducing the heat input in the generator.

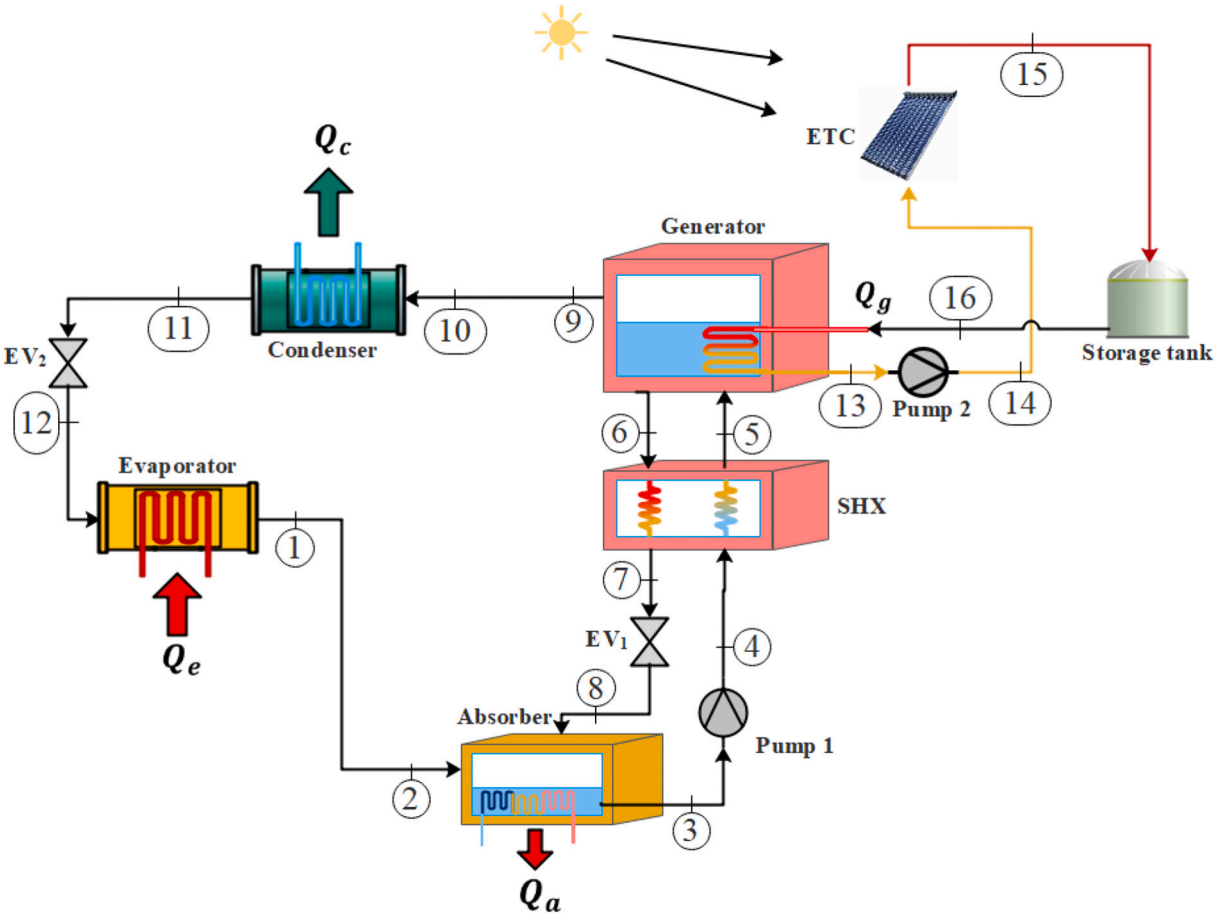


**Fig. 1.** Configuration of the basic single-stage solar absorption cooling system.

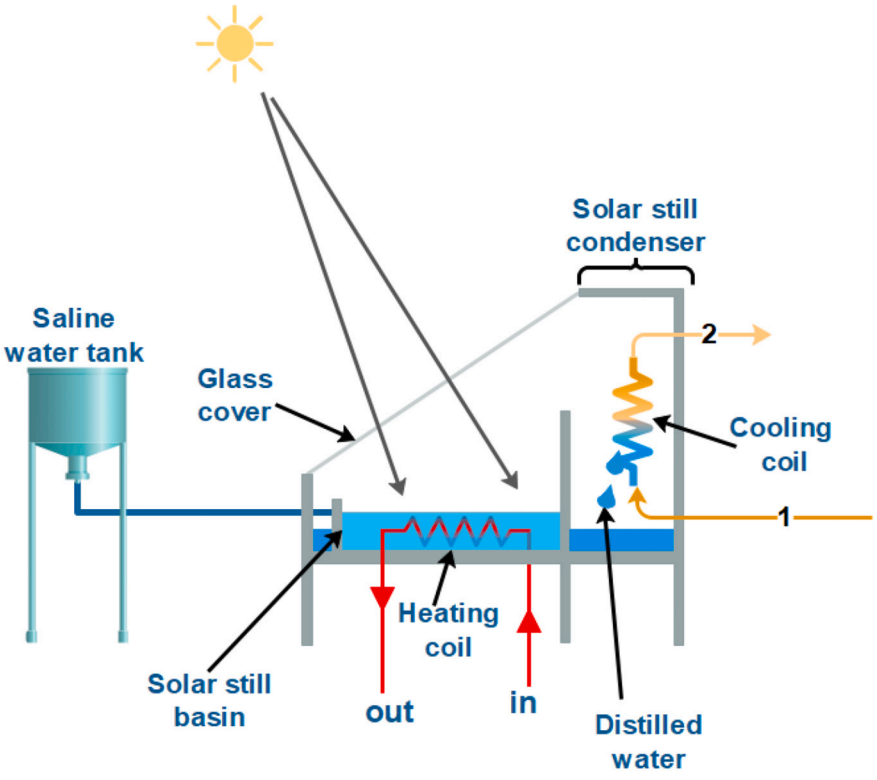


**Fig. 2.** Components of the basic solar still system.

The thermal energy is supplied to the generator by utilizing evacuated tube collectors (ETCs) with water as the heat transfer fluid (HTF). The ETCs can supply water with a temperature up to 105 °C. However, this temperature varies with the variation of solar radiation. So, a storage tank could be used to maintain a stable temperature at the inlet of the generator (state 16). The most common absorption systems utilize water/lithium-bromide ($H_2O$-LiBr) or ammonia/water ($NH_3$-$H_2O$) as refrigerant-absorbent pairs. $H_2O$-LiBr pair is used for cooling applications above 0 °C such as air-conditioning systems, and hence it is used in the present study as the refrigerant-absorbent pair.

Fig. 2 represents the configuration of the proposed solar still system. It consists of a single-slope solar still with an integrated condenser and a heating coil immersed in its basin. Without these coils, the solar still produces water by the following mechanism: the incident solar energy is absorbed by the saline water (in the basin) with a small fraction being reflected by the glass cover. The saline water utilizes the absorbed energy in the form of radiation, convection, and evaporation between the basin and the glass cover. The produced vapor is transferred (by concentration gradient) from the surface of the saline water and condenses on the inner surface of the glass cover. Usually, as the solar radiation increases, the evaporation rate will be higher than the condensation rate (due to the increase of the glass cover temperature), which causes the vapor to be trapped inside the available space between the basin and the glass cover. To address this issue, a condensation chamber is integrated into the still to increase the concentration gradient and to maintain the continuous evaporation-condensation process [48]. However, the productivity of the still is not considerably improved with the addition of the condensation chamber alone. Instead, in the present study, the still productivity will be improved significantly by enhancing the evaporation process (by a heating coil) and the condensation process (by a cooling coil) as shown in Fig. 2. The heating coil is powered by waste heat being recovered from the absorption system in three different configurations proposed by the authors in this paper. Also, the cooling coil absorbs the heat as part of the cooling load of the absorption system evaporator (in the three configurations). The next section explains these configurations in detail.

### 2.2. Proposed systems

The high temperature of the generated vapor of the refrigerant in the generator, necessitates the use of large condenser with high cooling capacity to condense the water vapor. However, if this vapor is directed to the basin of the solar still (as shown in Fig. 3), part of its heat will be absorbed and used to enhance the evaporation process. Furthermore, the cooling capacity of the condenser will be reduced, and as a result its size is reduced too. For convenience, this configuration is referred to as configuration 1 (S1). The second configuration (S2) is to enhance the evaporation process by the heating coil as shown in Fig. 4. In S2, the strong solution (rich in LiBr) passes through the heating coil then proceeds to the SHX. This way, the temperature of the weak solution (weak in LiBr, state 5) will be lower than that of the basic system (Fig. 1) and the load of the generator will be increased. However, the productivity of the still will efficiently be enhanced and the weak solution returns to the absorber with a similar temperature to the basic configuration. This maintains a suitable operating temperature for the absorber.

The third configuration (S3) is shown in Fig. 5. The heat transfer fluid leaves the generator at high temperature (state 13) suitable to be utilized to further enhance the evaporation process of the solar still. However, this increases the required area of the evacuated tube collectors (ETCs). It can be noted that the inlet fluid to the heating coil is different in each configuration. In S1, the inlet fluid is the vapor of the water (refrigerant). In S2, the inlet fluid is the strong solution of the ($H_2O$-LiBr) mixture. In S3, the inlet fluid is the water (HTF) in the liquid phase. However, the inlet temperature at the inlet of heating coil is approximately the same for all configurations. This implies that the properties of the inlet fluid will play major role in the determination of the best configuration. So, an accurate estimation model for the heat transfer coefficient inside the heating coil is developed as explained in

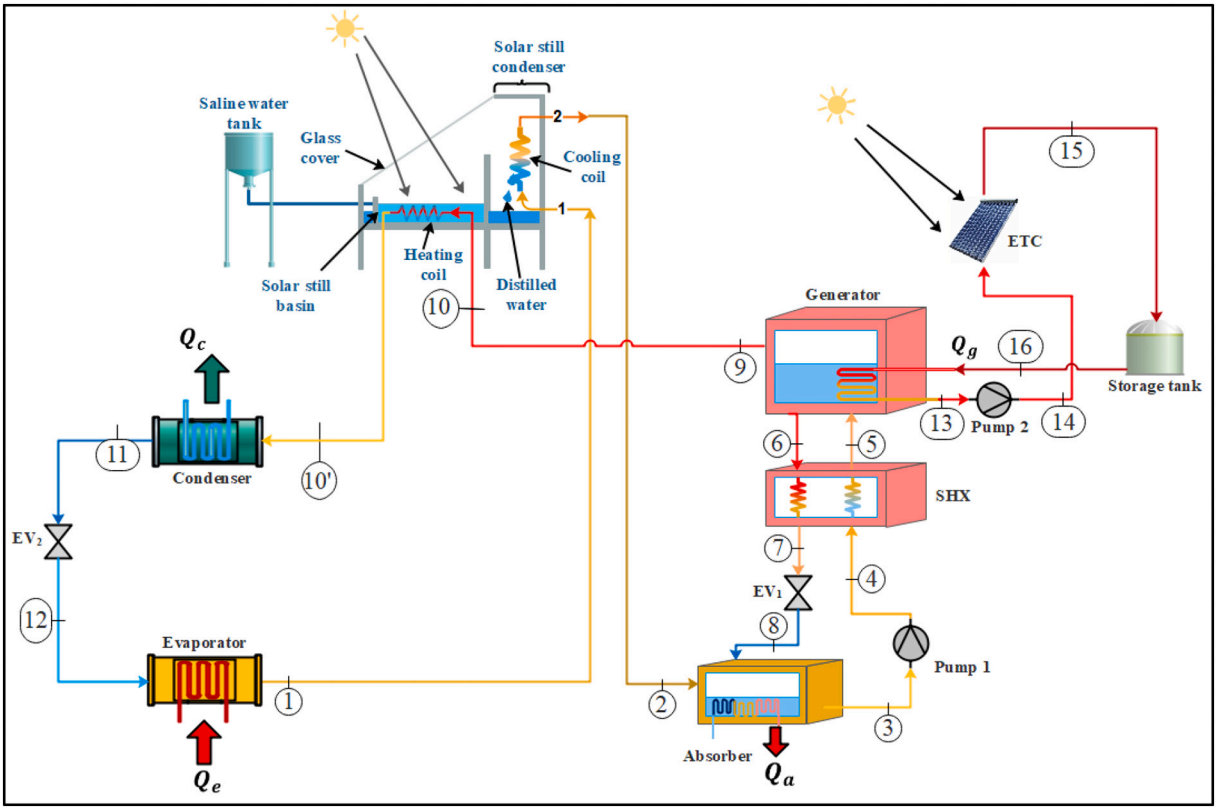


**Fig. 3.** Configuration S1, heat recovery from the refrigerant vapor leaving the generator.

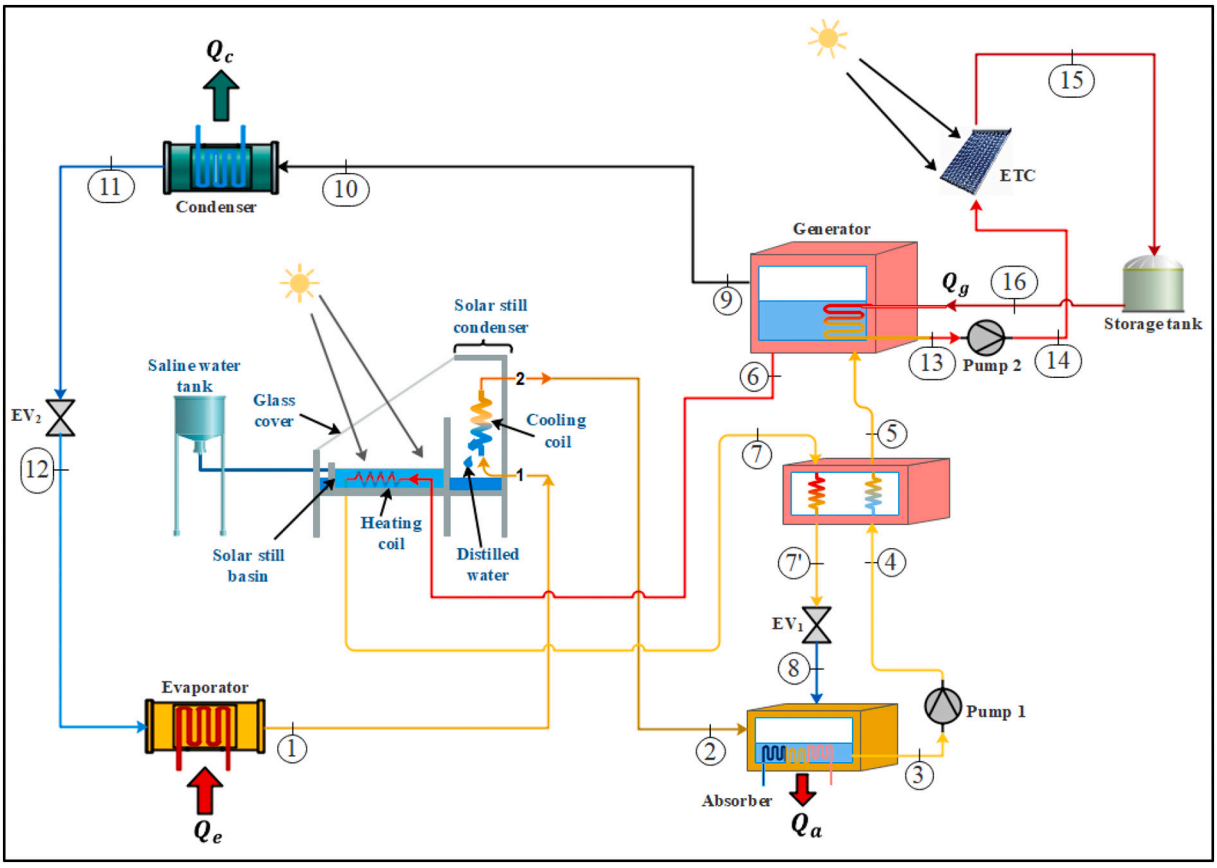


**Fig. 4.** Configuration S2, heat recovery from the strong solution leaving the SHX.

Section 3.

Table 1 illustrates the differences between the integrated configurations including the positions of the heating and cooling coils in the absorption system, temperatures and flow rates at the inlet and outlet of the heating coil, and the type of the fluid passes through the heating coli.

## 3. Thermodynamic model

### 3.1. Solar absorption cooling system model

Referring to Fig. 1, by applying energy, mass, and concentration balances to each component of the system, a thermodynamic model of the basic absorption system, with water/lithium bromide mixture as the working fluid, is developed with the following assumptions:

- Steady-state analysis.
- The variation of the kinetic and potential energies through each component is neglected.
- Pressure drop due to friction is neglected.

#### 3.1.1. Evaporator

At a refrigerant mass flow rate of $\dot{m}_r$, evaporator pressure $P_e$, and evaporator temperature of $T_e$, $Q_e$ (the cooling capacity) is given as:

$$Q_e = \dot{m}_r\,(h_1 - h_{12}) \tag{1}$$

where $h_1$ and $h_{12}$ are the specific enthalpies of the refrigerant (water) at the outlet and inlet of the evaporator, respectively.

#### 3.1.2. Absorber

The mass and concentration balances of the absorber are given as:

$$\dot{m}_2 + \dot{m}_8 = \dot{m}_3 \tag{2}$$

$$\dot{m}_8 x_8 = \dot{m}_3 x_3 \tag{3}$$

where $\dot{m}_2 = \dot{m}_1 = \dot{m}_r$, $\dot{m}_8$ is the mass flow rate of the strong solution (rich in LiBr), and $\dot{m}_3$ is the mass flow rate of the weak solution (weak in LiBr). $x_8$ and $x_3$ are solution concentrations of strong and weak solutions, respectively. The heat released through the absorption process is given as:

$$Q_a = \dot{m}_2 h_2 + \dot{m}_8 h_8 - \dot{m}_3 h_3 \tag{4}$$

#### 3.1.3. Solution pump

The consumed power by the solution pump (Pump 1 in Fig. 1) is expressed in terms of the solution enthalpies at states 3 and 4 as given in Eq. (5). Also, it is expressed in terms of the specific volume and pressure difference as given in Eq. (6).

$$\dot{W}_{p1} = \dot{m}_3 (h_4 - h_3) \Big/ \eta_{p1} \tag{5}$$

$$\dot{W}_{p1} = \dot{m}_3 v_3 (P_4 - P_3) \Big/ \eta_{p1} \tag{6}$$

$P_4$ and $P_3$ are the high and low pressures of the absorption systems. $P_4$ is the operating pressure of the generator and the condenser and defined as the saturation pressure of the water at the condenser temperature $P_4 = P_{sat@T_c}$. $P_3$ is the operating pressure of the absorber and the evaporator and is defined as the saturation pressure of the water at the evaporator temperature $P_3 = P_{sat@T_e}$.

#### 3.1.4. Generator

The mass and concentration balances of the generator are expressed

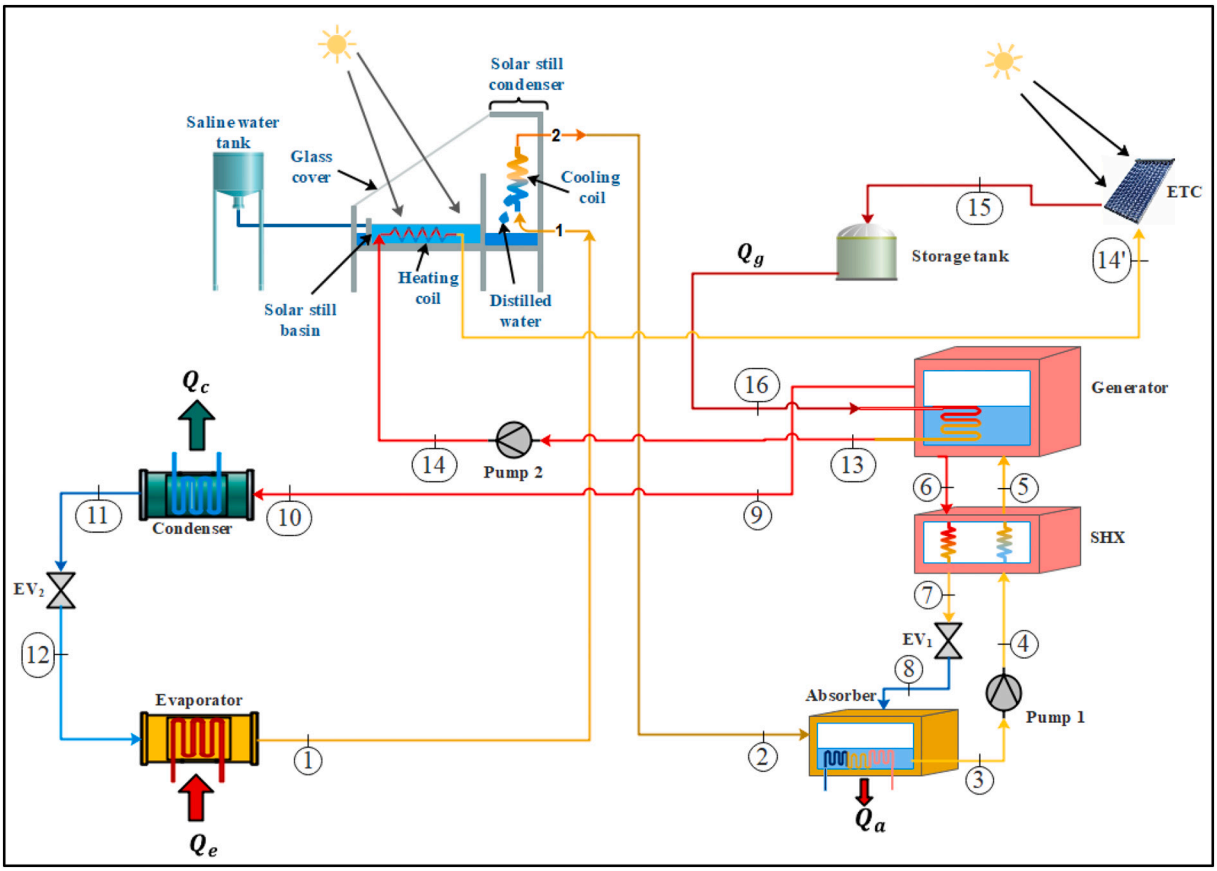


**Fig. 5.** Configuration S3, heat recovery from the HTF leaving the generator.

**Table 1**
Major differences between the proposed configurations.

| System | Position of the heating coil | Position of the cooling coil | Fluid passes through the heating coil | $T_{hc,\ in}$ | $T_{hc,\ out}$ | $\dot{m}_{hc}$ |
|---|---|---|---|---|---|---|
| S1 | At the exit of the generator (water vapor stream) | At the exit of the evaporator | Water vapor | $T_{10}$ | $T_{10'}$ | $\dot{m}_{10}$ |
| S2 | At the exit of the generator (strong solution stream) | At the exit of the evaporator | $H_2O$-LiBr mixture | $T_6$ | $T_7$ | $\dot{m}_6$ |
| S3 | At the exit of the generator (HTF stream) | At the exit of the evaporator | Liquid water (HTF) | $T_{14}$ | $T_{15}$ | $\dot{m}_{14}$ |

as:

$$\dot{m}_5 = \dot{m}_6 + \dot{m}_9 \tag{7}$$

$$\dot{m}_5 x_5 = \dot{m}_6 x_6 \tag{8}$$

And the absorbed heat in the generator is given as:

$$Q_g = \dot{m}_6 h_6 + \dot{m}_9 h_9 - \dot{m}_5 h_5 \tag{9}$$

### 3.1.5. Solution heat exchanger (SHX)

The SHX recovers the heat from the strong solution (states 6–7 in the basic, S1 and S3 or states 7–7′ in S2) by the weak solution (states 4–5). The governing equations of the counter-flow heat exchanger are used as a model for the SHX as flows:

$$Q_r = \dot{m}_6 c_{p,ss} \ (T_6 - T_7) \tag{10}$$

$$Q_r = \dot{m}_5 \ c_{p,ws} \ (T_5 - T_4) \tag{11}$$

$$\varepsilon_{SHX} = \frac{Q_r}{Q_{r,max}} = \frac{Q_r}{C_{min}(T_6 - T_4)} \tag{12}$$

$$C_{min} = C_{ss} \tag{13}$$

where $Q_r$ is the recovered heat by the SHX, $\varepsilon_{SHX}$ is the effectiveness of the SHX, $C_{ss}$ is the heat capacity rate of the strong solution. The heat capacity rate is given as the product of the mass flow rate by the specific heat of each solution as:

$$C_{ss} = \dot{m}_6 \ c_{p,ss} \tag{14}$$

### 3.1.6. Condenser

The cooling load of the condenser is calculated as:

$$Q_c = \dot{m}_{10}(h_{10} - h_{11}) \tag{15}$$

### 3.1.7. Expansion valves

The governing equations of the expansion valves ($EV_1$ and $EV_2$ in Fig. 1) are needed to finalize the required equations of the absorption cycle components and are expressed as:

$$h_7 = h_{8,} \ and \ h_{11} = h_{12} \tag{16}$$

It can be noted that $\dot{m}_3 = \dot{m}_4 = \dot{m}_5 = \dot{m}_{ws}; \dot{m}_6 = \dot{m}_7 = \dot{m}_8 = \dot{m}_{ss}; \dot{m}_9 = \dot{m}_{10} = \dot{m}_{11} = \dot{m}_{12} = \dot{m}_1 = \dot{m}_r$.

### 3.1.8. Equations of the proposed configurations

In the proposed configurations, the cooling coil of the solar still is considered as an additional load on the evaporator. It is inserted between states 2 and 3 in all configurations. So, the absorbed heat from the

vapor of the solar still water by the cooling coil is expressed as:

$$Q_{cc} = \dot{m}_1 c_{p,r}(\Delta T_{cc}), \Delta T_{cc} = T_2 - T_1 \quad (17)$$

where $\Delta T_{cc}$ is the temperature difference of the refrigerant (water) across the cooling coil.

The heat added to the saline water from the absorption system can be expressed as:

$$Q_{hc} = U_{hc}\, A_{hc}\, LMTD \quad (18)$$

where $U_{hc}$ is the overall heat transfer coefficient between the working fluid of the absorber cycle and the saline water, $A_{hc}$ is the surface area of the heating coil ($A_{hc} = \pi D_{hc} L_{hc}$), and $LMTD$ is the log mean temperature difference.

Neglecting the thermal resistance of the heating coil material, $U_{hc}$ is given in terms of the heat transfer coefficients of the forced convection $h_{hc,\,i}$ and the free convection $h_{hc,\,o}$ (see Fig. 6) as:

$$U_{hc} = \frac{1}{\frac{1}{h_{hc,i}} + \frac{1}{h_{hc,o}}} \quad (19)$$

Due to the dependency of the internal heat transfer coefficient on the nature of the flowing fluid of each configuration, it is necessary to define it in terms of Reynolds and Nusselt numbers as follows:

$$Re_{hc} = \frac{4\dot{m}_{hc}}{\pi \mu_{hc} D_{hc}} \quad (20)$$

$$Nu_{hc} = \frac{h_{hc,i} D_{hc}}{k_{hc}} = 0.023 \times Re_{hc}^{0.8} \times Pr_{hc}^{0.3} \quad (21)$$

where $Pr$ is the Prandtl number of the fluid in the heating coil.

Now, the heat transferred by the heating coil to the saline water is expressed in terms of the mass flow rate, specific heat, and temperature difference of the fluid in each configuration. The mass flow rate and inlet and outlet temperatures of the heating coil are unique parameters for each configuration. In S1 ($\dot{m}_{hc} = \dot{m}_{10}$, $T_{hc,\,in} = T_{10}$ and $T_{hc,\,out} = T_{10'}$), in S2 ($\dot{m}_{hc} = \dot{m}_6$, $T_{hc,\,in} = T_6$ and $T_{hc,\,out} = T_7$), and in S3 ($\dot{m}_{hc} = \dot{m}_{14}$, $T_{hc,\,in} = T_{14}$ and $T_{hc,\,out} = T_{14'}$). Therefore, in S1 (Fig. 3), the fluid inside the coil is the water vapor and the $Q_{hc}$ is given as:

$$Q_{hc} = \dot{m}_{10} c_{p,10}(T_{10} - T_{10'}) \quad (22)$$

In configuration 2 (Fig. 4), the strong solution is the fluid flow inside the heating coil. In this configuration,

$$Q_{hc} = \dot{m}_6 c_{p,ss}(T_6 - T_7) \quad (23)$$

In configuration 3 (Fig. 5), the hot liquid water is the fluid flows inside the heating coil. In this configuration,

$$Q_{hc} = \dot{m}_{14} c_{p,14}(T_{14} - T_{14'}) \quad (24)$$

### 3.2. Modelling the solar still system

The solar still thermodynamic model is adapted from the previous authors' work [48] and provided here for clarity and completeness. The assumptions are:

- The solar still system operates under steady-state conditions.
- The heat losses across the walls and the basin of the still are negligible.

Referring to Fig. 7, the energy conservation principle (ECP) is applied to the saline water and on the glass cover to get the governing equations of the still. Applying the ECP to the saline water:

$$Q_{sun} + Q_{hc} - \left(Q_{ev,sw-gl} + Q_{c,sw-gl} + Q_{r,sw-gl}\right) = 0 \quad (25)$$

where $Q_{sun}$ is the rate of the solar energy incident on the saline water from the sun. It is given as:

$$Q_{sun} = \tau_{gl} \alpha_w A_{sw} G \quad (26)$$

$Q_{hc}$ is the heat transferred to the saline water from the absorption system by the heating coil (as discussed in Section 3.1.7) and set as $Q_{hc} = 0$ for the basic solar system calculations. $Q_{r,\,sw-g}$ is the rate of the radiative energy loss between the saline water and the glass cover of the still. It is given as [49]:

$$Q_{r,sw-gl} = \varepsilon_{sw-gl} \sigma A_{sw} \left(T_{sw}^4 - T_{gl}^4\right) \quad (27)$$

$Q_{c,\,sw-gl}$ is the rate of the energy loss from the saline water to the inside air by convection. It is given as [49]:

$$Q_{c,sw-gl} = h_{c,sw-gl} A_{sw} \left(T_{sw} - T_{gl}\right) \quad (28)$$

$Q_{ev,\,sw-gl}$ is the rate of the energy consumed to evaporate the saline water from the basin to the inside air and condensing chamber. It is given as [49]:

$$Q_{ev,sw-gl} = h_{ev,sw-gl} A_{sw} \left(T_{sw} - T_{gl}\right) \quad (29)$$

where $h_{ev,\,sw-gl}$ is the vaporization coefficient of saline water given as [50]:

$$h_{ev,sw-gl} = 16.273 \times 10^{-3} \times h_{c,sw-gl} \times \left[\frac{P_{sw} - P_{gl}}{T_{sw} - T_{gl}}\right] \quad (30)$$

$P_{sw}$, $P_{gl}$ are the effective saturated vapor pressure of the freshwater vapor at the saline water temperature $T_{sw}$ and glass cover temperature $T_{gl}$, respectively, given as [51]:

$$P_{sw} = exp\left[25.317 - \left(\frac{5144}{T_{sw}}\right)\right] \quad (31)$$

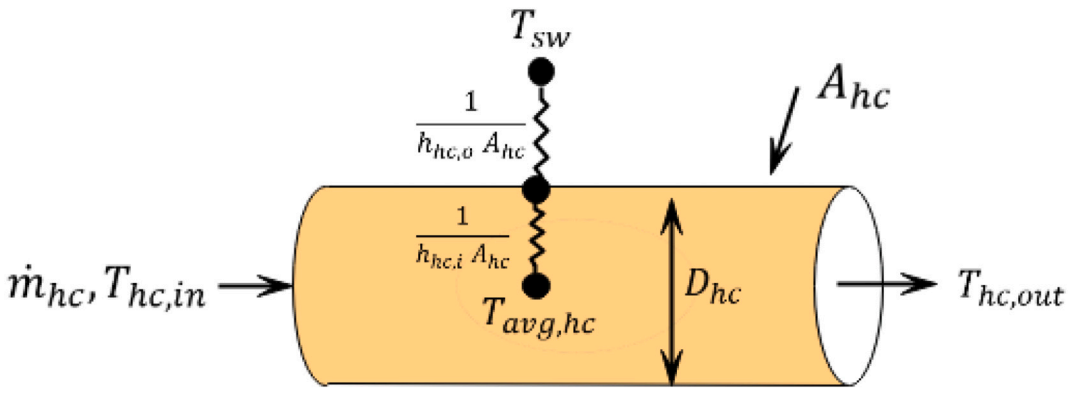


**Fig. 6.** Thermal model of the heating coil.

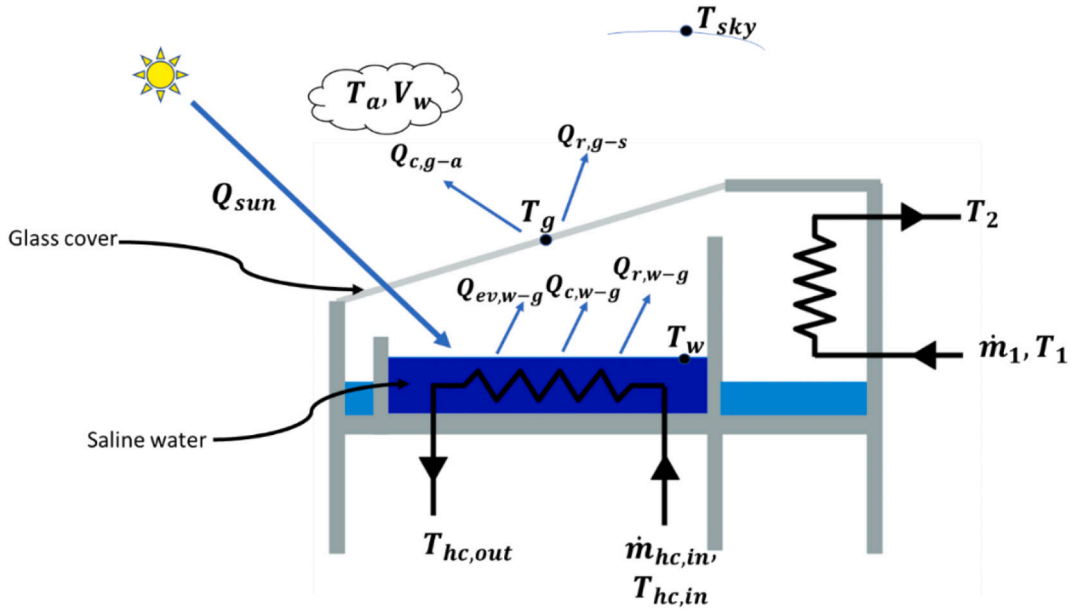


**Fig. 7.** Schematic diagram of the heat transfer processes of the still.

$$P_{gl} = exp\left[25.317 - \left(\frac{5144}{T_{gl}}\right)\right] \tag{32}$$

The $h_{c,\,sw-gl}$ is the convective heat transfer coefficient between saline water and glass cover given as [51]:

$$h_{c,sw-gl} = \frac{k_v}{L_v} \times C(Gr \cdot Pr)^n \tag{33}$$

$$Gr = \frac{\beta g L_v^3 \rho_v^2 \Delta T}{\mu_v^2} \tag{34}$$

$$Pr = \frac{\mu_v c_{p,v}}{k_v} \tag{35}$$

$$\Delta T = (T_{sw} - T_{gl}) + \frac{(P_{sw} - P_{gl})(T_{sw})}{(268.9 \times 10^3 - P_{sw})} \tag{36}$$

Applying the ECP on the glass cover and the condensing chamber of the still gives:

$$Q_{ev,sw-gl} + Q_{c,sw-gl} + Q_{r,sw-gl} - (Q_{cc} + Q_{c,gl-a} + Q_{r,gl-sky}) = 0 \tag{37}$$

where $Q_{cc}$ is the absorbed heat by the cooling coil (given in Eq. (17)) and set as $Q_{cc} = 0$ for the basic solar system calculations. $Q_{r,\,gl-sky}$ is the rate of the energy loss by radiation from the glass cover to the sky [49]:

$$Q_{r,gl-sky} = \varepsilon_{g-sky} \sigma A_{gl} \left(T_{gl}^4 - T_{sky}^4\right) \tag{38}$$

where $T_{sky}$ is the effective temperature of the sky and expressed as [48]:

$$T_{sky} = 0.0552 \times (T_a)^{1.5} \tag{39}$$

The rate of the convention energy loss between glass cover and ambient air $Q_{c,\,gl-a}$ is expressed as [49]:

$$Q_{c,gl-a} = h_{c,gl-a} A_{gl} (T_g - T_a) \tag{40}$$

where $h_{c,\,gl-a}$ is the convective heat transfer coefficient between the glass cover and ambient air, given as [48]:

$$h_{c,gl-a} = 2.8 + 3.0 \times V_{wind} \tag{41}$$

The per hour (for a day) amount of the produced distilled is:

$$m_{distilled} = \sum_i^j \left(\frac{Q_{ev,sw-gl,i}}{h_{fg,v,i}}\right) \times 3600 \tag{42}$$

where i to j is the hour in the day when the sun is shining (7:00, 8:00, …, …, 17:00) and $h_{fg,\,v}$ is water enthalpy of vaporization.

### 3.3. Performance indicators of the integrated system

The proposed system is composed of a single-effect absorption system and a single slope solar still system. This implies that there are two useful products: freshwater and cooling effect. The performance of the solar still expressed in terms of its efficiency is given as [48]:

$$\eta_{ss} = \frac{Q_{ev,sw-gl}}{G \times A_{sw} + Q_{hc}} \tag{43}$$

The coefficient of performance (COP) for the absorption cooling system is given as [52,53]:

$$COP = \frac{Q_e}{Q_g + \dot{W}_{p1} + \dot{W}_{p2}} \tag{44}$$

The energy performance of the integrated system combines both the distilled water evaporation energy and the cooling effect since they are produced by the same input energy. It is introduced to reveal the contribution of each configuration in the improvement of the solar still productivity expressed as [53]:

$$EP = \frac{Q_e + \dot{m}_{sw} h_{fg}}{\left(Q_{ETC} + \dot{W}_{p1} + \dot{W}_{p2}\right) + Q_{sun}} \tag{45}$$

where

$$Q_{ETC} = GA_{ETC} \tag{46}$$

Finally, the performance of the solar evacuated tube collectors is expressed in terms of their efficiency $\eta_{ETC}$, which is given by the Hottel-Whillier equation as [54]:

$$\eta_{ETC} = F_R(\tau\alpha) - F_R U_L \left(\frac{T_{coll,in} - T_a}{G}\right) \tag{47}$$

where, $F_R$ is the heat removal factor, $\tau\alpha$ is the absorption-transmittance

product of the glass cover and tube of the ETCs, $T_{coll,\ in}$ is the temperature at the inlet of the ETCs (sate 14 in Fig. 1), $T_a$ is the ambient temperature, and $G$ is the solar radiation intensity.

### 3.4. Design point and validation

Table 2 shows the design values and ranges of the input parameters. The generator temperature range was selected to be within the proofed capabilities of the evacuated tube collectors. The absorber and condenser temperature ranges were chosen based on the cooling method (wet cooling by water or dry cooling by air). The evaporator temperature range was selected to fit the air conditioning applications. Table 3 provides the thermodynamics properties at the state points of the basic absorption system (Fig. 1) at the design point specifications. The data of the $H_2O$/LiBr mixture and water vapor are obtained from the external library of the Engineering Equation Solver (EES) and the modelling equations were solved by EES. Fig. 8 shows the solution procedures of the integrated absorption-solar still system. For validation purposes, the results of the basic absorption model are compared with experimental work conducted by Lizarte et al. [55] as shown in Table 4. The average error for four sets of operating parameters is 5.5%, which is within the experimental uncertainty. Also, the solar still model is validated by comparison with experimental data reported by Madiouli et al. [56] as shown in Table 5, where the percentage difference, given the differences between the two systems, is considered reasonable (3.33%). The deviation percent shown in Table 4 and Table 5 is defined as: 100 * | Expermental value (Ref.) − Theoretical value (present study)| / Expermental value (Ref.).

## 4. Results and discussion

The effects of the operational parameters on the system performance are investigated in this section and an estimation for the distilled water cost is presented.

**Table 2**
Typical operating conditions of the proposed system.

| Parameter | Design value (range) |
|---|---|
| *Absorption system* | |
| Outlet temperature from the ETCs, $T_{16}$ °C | 100 |
| Generator temperature, $T_6$ °C | 90 (75–95) |
| Absorber temperature, $T_3$ °C | 35 (30–50) |
| Condenser temperature, $T_{11}$ (°C) | 35 (30–50) |
| Evaporator temperature, $T_1$ (°C) | 5 (5–10) |
| Cooling capacity, $Q_e$ (kW) | 20 |
| Effectiveness of the solution heat exchanger, $\varepsilon_{SHX}$ (%) | 80 |
| Pump isentropic efficiency 1, $\eta_{p1}$ (%) | 85 |
| Solar collector optical efficiency, $F_R(\tau\alpha)$ | 0.79 |
| Loss coefficient of the solar collectors, $F_R U_L$ (W/m$^2$-°C) | 5.2 |
| The temperature difference across the cooling coil $\Delta T_{cc}$ (°C) | 5.0 |
| The diameter of the heating coil, $D_{hc}$ (cm) | 7.0 |
| Length of the heating coil, $L_{hc}$ (m) | 10.0 |
| Power consumed by pump 2 | 8.36 kW/kg |
| *Solar still system* | |
| Solar radiation flux, $G$ (W/m$^2$) | 500 (300–1000) |
| Wind speed, $V_{wind}$ (m/s) | 3 |
| Ambient temperature, $T_a$ (°C) | 35 |
| Saline water area, $A_{sw}$ (m$^2$) | 1 |
| Glass cover area, $A_{gl}$ (m$^2$) | 1 |
| Transmissivity of the glass cover, $\tau_{gl}$ | 0.95 |
| The absorptivity of saline water, $\alpha_{sw}$ | 0.90 |
| Average distance between the saline water and the glass cover, $L_v$ (m) | 0.5 |
| Heat transfer coefficient outside the heating coil, $h_{hc,\ o}$ (W/m$^2$-°C) | 0.3 |
| Depth of the basin water, m | 0.2 |
| Emissivity of the glass cover, $\varepsilon_{g-sky}$ | 1 |
| Emissivity of the saline water, $\varepsilon_{sw-gl}$ | 1 |
| Number of sunshine hours | 10 |

**Table 3**
Thermodynamic properties at each state of the basic absorption system.

| State point | Fluid | T (°C) | P (kPa) | X (%) | $\dot{m}$ (kg/s) | h (kJ/kg) |
|---|---|---|---|---|---|---|
| 1 | Water vapor | 5 | 0.873 | 0.00 | 0.008463 | 2510.00 |
| 2 | Water vapor | 5 | 0.873 | 0.00 | 0.008463 | 2510.00 |
| 3 | Water/LiBr | 35 | 0.873 | 55.28 | 0.057753 | 85.29 |
| 4 | Water/LiBr | 69.34 | 5.627 | 55.28 | 0.057753 | 85.29 |
| 5 | Water/LiBr | 81.77 | 5.627 | 55.28 | 0.057753 | 181.50 |
| 6 | Water/LiBr | 90 | 5.627 | 64.77 | 0.049290 | 239.60 |
| 7 | Water/LiBr | 73.47 | 5.627 | 64.77 | 0.049290 | 210.00 |
| 8 | Water/LiBr | 54.25 | 0.873 | 64.77 | 0.049290 | 210.00 |
| 9 | Water vapor | 90 | 5.627 | 0.00 | 0.008463 | 2669.00 |
| 10 | Water vapor | 90 | 5.627 | 0.00 | 0.008463 | 2669.00 |
| 11 | Water liquid | 35 | 5.627 | 0.00 | 0.008463 | 146.60 |
| 12 | Vapor-liquid water | 5 | 5.627 | 0.00 | 0.008463 | 146.60 |
| 13 | Water liquid | 95 | 100 | – | 1.114 | 398.00 |
| 14 | Water liquid | 95 | 500 | – | 1.114 | 398.30 |
| 15 | Water liquid | 105 | 500 | – | 1.114 | 440.50 |
| 16 | Water liquid | 100 | 500 | – | 1.114 | 419.40 |

| Outputs | |
|---|---|
| Cooling capacity, $Q_e$ kW | 20.00 |
| Heat absorbed by the generator, $Q_g$ kW | 23.92 |
| The heat released by the absorber, $Q_a$ kW | 22.60 |
| Heat rejected by the condenser, $Q_c$ kW | 21.34 |
| Heat recovered by the solution heat exchanger, $Q_r$ kW | 2.07 |
| Power consumed by the pump 1, $W_{p1}$ kW | 0.171 |
| Power consumed by the pump 2, $W_{p2}$ kW | 0.183 |
| Coefficient of performance, COP | 0.83 |
| The required area of the ETCs, $A_{ETC}$ m$^2$ | 76.83 |

Before proceeding to the discussion of the effects of the major operating conditions, it is important to give an insight on the significance of integrating the cooling coil to the basic solar still is S1, S2, and S3 which enhances the condensation process of the distilled water (process 1–2 in Figs. 3 to 5). As shown in Fig. 9, the distilled water linearly increases with the increase of the temperature difference across the cooling coil. At the design point conditions shown in Table 2 with no cooling coil ($\Delta T_{cc} = 0$), the still productivity is 4.35 kg/day. With temperature difference of 10 °C across the cooling coil of the proposed configurations, the still productivity increases to 8.85 kg/day in S1, 10.29 kg/day in S2, and 11.64 kg/day in S4. However, larger temperature difference across the cooling coil dictates larger cooling load for the absorber and negatively affects the COP of the absorption system. Therefore, the temperature difference across the cooling coil was fixed at 5 °C to improve the condensation process of the distilled water with negligible effect on the COP of the absorption system.

### 4.1. Generator temperature effect

Fig. 10 shows the generator temperature effect on the COP, EP, and distilled water of the proposed systems. It should be mentioned that the "Basic" configuration means that there is no integration between the basic absorption system (Fig. 1) and the basic solar still system (Fig. 2).

As shown in Fig. 10(a), the COP of the second configuration S2 is lower than that of the other configurations (notice that in Fig. 10, the curves of the Basic, S1 and S3 configurations are on top of each other). This means that the insertion of the heating coil before the SHX affects the performance of the absorption system. It reduces the COP by 6% at low generator temperatures to 2% at high generator temperatures. Furthermore, it is noted that the COP increases with the generator temperature up to an optimum value then reduces with a further increase in the generator temperature except for S2. However, the variation of the COP with the generator temperature is <0.004 and seems to be maintained at 0.85. Moreover, the COPs of the basic, S1, and S3 are identical since the evaporator and generator loads are the same for all of them. However, the required area for S3 is higher than of the basic and

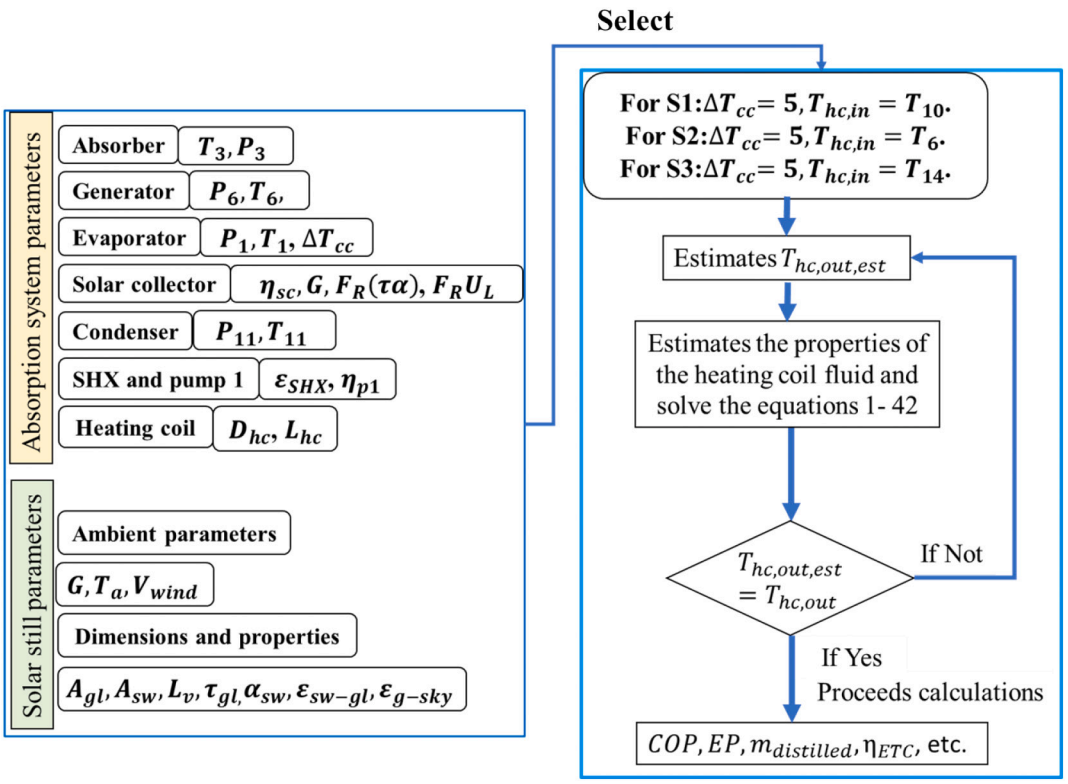


**Fig. 8.** Solution procedures.

**Table 4**
Validation of the solar absorption cooling model.

| Study no. | Evaporator temp. °C | Absorber temp. °C | Generator temp. °C | Condenser temp. °C | COP [55] | COP [present study] | Deviation (%) |
|---|---|---|---|---|---|---|---|
| 1 | 11.10 | 39.2 | 96.5 | 42.7 | 0.60 | 0.61 | 1.6 |
| 2 | 11.20 | 41.9 | 99.4 | 44.2 | 0.63 | 0.60 | 4.7 |
| 3 | 11.00 | 43.10 | 102.6 | 45.0 | 0.65 | 0.63 | 3.1 |
| 4 | 10.8 | 43.5 | 102.8 | 45.2 | 0.70 | 0.68 | 2.8 |

**Table 5**
Validation of the solar still model.

| Parameter | Study 3 [56] | Present study | Deviation (%) |
|---|---|---|---|
| $G$, W/m$^2$ | 957 | 975 | Input |
| $T_a$, K | 300 | 300 | Input |
| $V_{wind}$, m/s | 3 | 3 | Input |
| $A_{gl}$, m$^2$ | 1 | 1 | Input |
| $A_{sw}$, m$^2$ | 1 | 1 | Input |
| $\eta_{ss}$, % | 22.00 | 23.02 | 4.63 |
| $m_{distilled}$, kg/m$^2$-h | 0.60 | 0.62 | 3.33 |

S1 (to maintain proper temperatures at states 16 and 13). Also, the condenser size of the basic and S3 is larger than of S1.

The definition of energy performance (Eq. (45)) was introduced to evaluate the contribution of each configuration in the heating and cooling enhancement of the solar still (HCE) system. The cooling enhancement is the same for all configurations (S1, S2 and S3) while the heating enhancement is different. As shown in Fig. 10(b), the EP of S3 is higher than of S2 and S1. Moreover, the EP of S2 is higher than the basic configuration at generator temperature higher than 90 °C. This returns to that the generator temperature higher than 90 °C is not preferable for single stage absorption systems. The EP of the basic configuration corresponds to its COP since it has no contribution to the enhancements of cooling and heating of the solar still system. The EPs of S3 and S1 are higher than their COP by 2.0%.

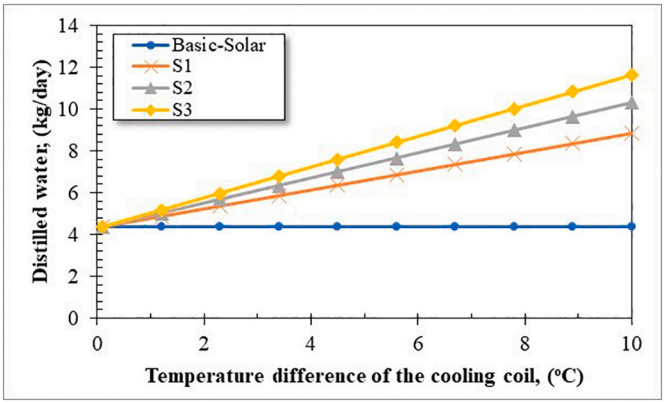


**Fig. 9.** Effect of the temperature difference of the cooling coil on production rate of distilled water.

While S2 configuration reduces the COP of the absorption system, it improves the still productivity better than S1 (see Fig. 10(c)). This means that the heating enhancement of S2 is higher than of S1 (by about 16%). However, the COP of S1 is higher than of S2 (only by 2.5%). Moreover, in S3 the still productivity is the highest. However, S1 improves the still productivity without affecting the COP of the absorption system and no effect on the area of the evacuated tube collectors (ETCs).

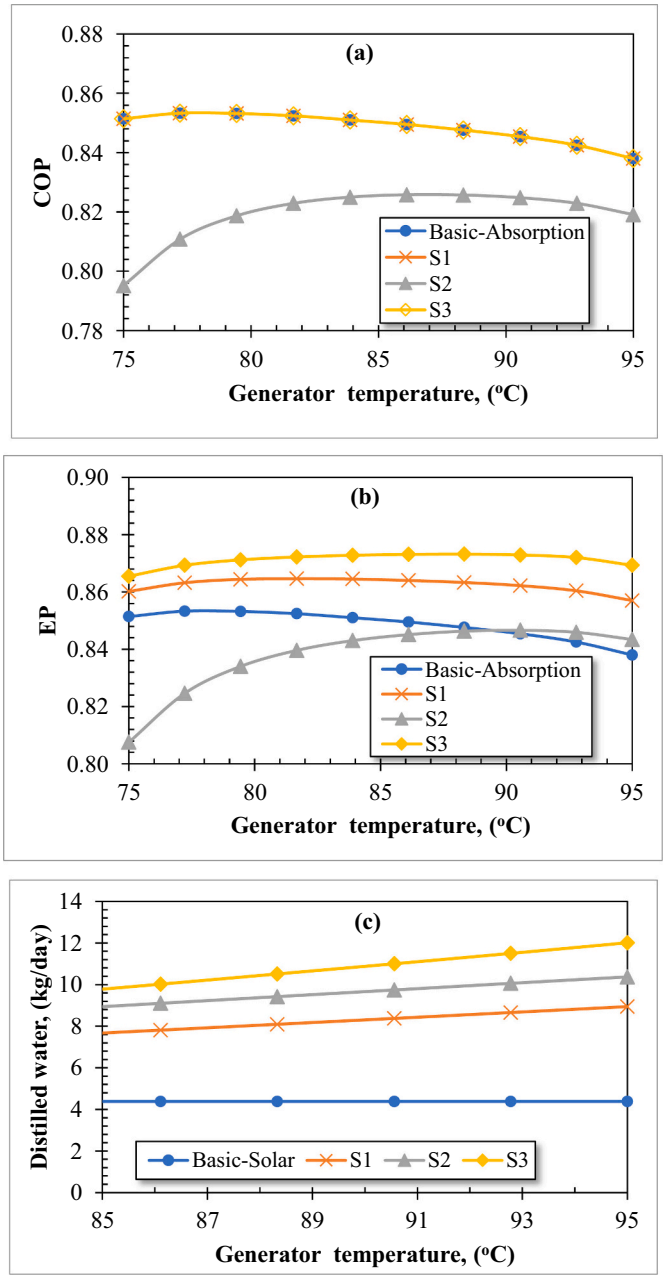


**Fig. 10.** Generator temperature effect on (a) COP, (b) EP, and (c) distilled water of the proposed system. Note: In Fig. 9(c), the amount of the distilled water of the basic solar system does not change with the variation of the generator temperature and plotted here for comparison purposes.

Furthermore, S1 reduces the capacity of cooling of the condenser since the solar still works as a pre-cooler for the water vapor before it passes through the condenser (See Fig. 3).

Comparing the still productivity in each configuration relative to the basic configuration (solar still alone), it can be noted that the improvement achieved by S1 is 104.1%, by S2 is 136.7%, and by S3 is 173.9%.

Fig. 11 shows the performance of the S2 in two different versions. The first one is the insertion of the heating coil instead of the SHX. The second one is the insertion of the heating coil cascaded with the SHX. In both cases, the COP and EP of the second version is better than the first one. It can be concluded that the first case improves the still productivity higher than the second one since more heat is added to the basin of the still. However, the elimination of the SHX increases the generator load

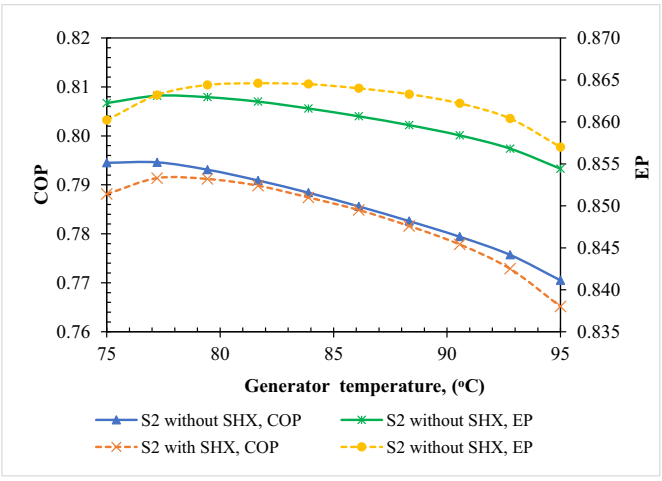


**Fig. 11.** Comparison of the S2 performance with and without SHX.

which affects both the COP and the EP more than the improvement in the solar still productivity. So, in this work, the second case is selected for further discussion.

### 4.2. Absorber temperature effect

Fig. 12 shows the effects of the absorber temperature on the COP, EP, and distilled water of the proposed configurations. In contrast to the generator temperature, the COP of the absorption system decreases with the increase of the absorber temperature. This is attributed to the decrease of the refrigerant solubility at higher absorber temperature. This decrease being sharper at temperatures higher than 40 °C as shown in Fig. 12(a). Similar to the generator temperature, the COP of S2 is lower than other configurations. Also, the EP of S3 is higher than of S1, S2, and basic configurations (Fig. 12(b)). The EP of S2 at absorber temperature <35 °C is slightly higher than of the basic configuration. This means that the improvement of the still productivity is higher than the improvement of the COP of S2 at lower absorber temperature. Regarding the productivity of the still, only S2 increases the still productivity with the increase of the absorber temperature (Fig. 12(c)). This is due to the increase of the heat recovered by the solar still basin since the flow rate of the strong solution at state 6 increases with the absorber temperature. It is noted that the effect of the condenser temperature is similar to the absorber temperature. That is the COP of the absorption system decreases with the increase of the condenser temperature. For better performance, the heat released from the absorber has to be absorbed by an external cooling process. The cooling process can be implemented by using dry air or cooling towers. However, utilizing cooling towers is more efficient for two reasons. First, the cooling by water at a temperature of 30 °C yields the highest COP (0.86) of the absorption system as shown in Fig. 12(a). Second, the cooling capacity could be controlled by adjusting the mass flow rate of the cooling water.

### 4.3. Effect of evaporator temperature

Fig. 13 shows the effects of the evaporator temperature on the COP, EP, and distilled water of the studied configurations. In air cooling applications, the chilled water enters the evaporator at a temperature of 12 °C; the evaporator temperature was varied within the range 5 °C to 10 °C. Furthermore, in the absorption system that utilizes water as a refrigerant, the evaporator temperature is set within this range to avoid the crystallization problem. As the evaporator temperature increases, with fixed cooling capacity, the mass flow rates of the refrigerant and absorbent decrease, which reduces the heating load of the generator and linearly increases the COP of the system. Due to this relationship, the

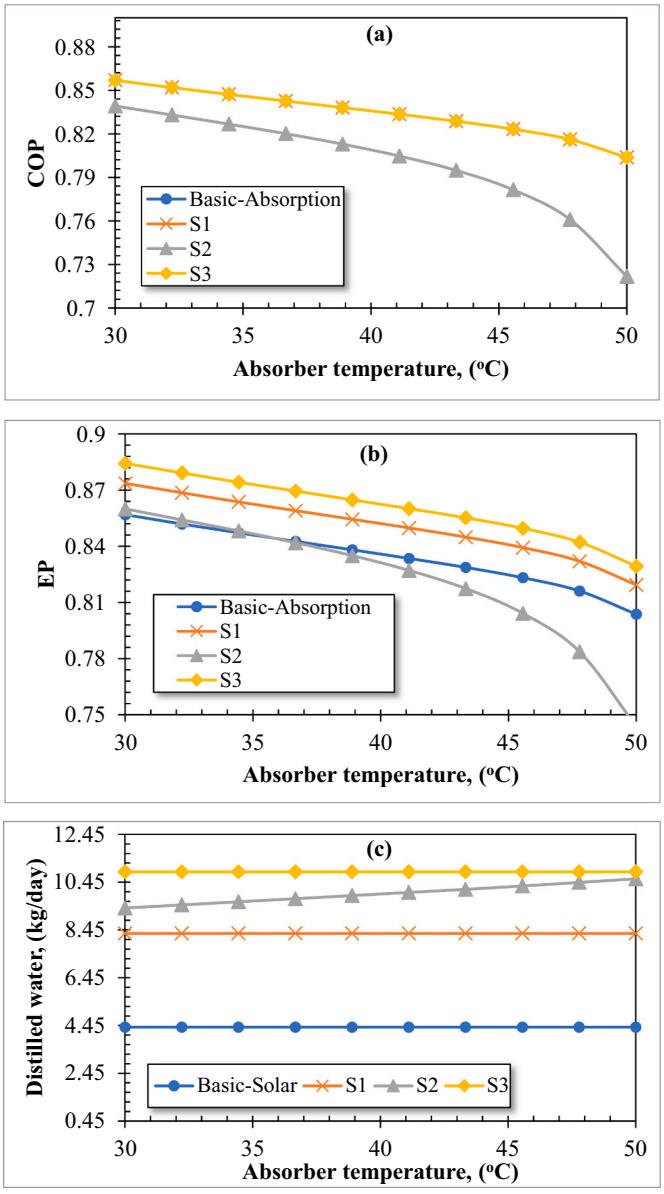


**Fig. 12.** Effect of the absorber temperature on (a) COP, (b) EP, and (c) distilled water of the proposed systems. Note: In (c), the amount of the distilled water of the basic solar system does not change with the variation of the absorber temperature and plotted here for comparison purposes.

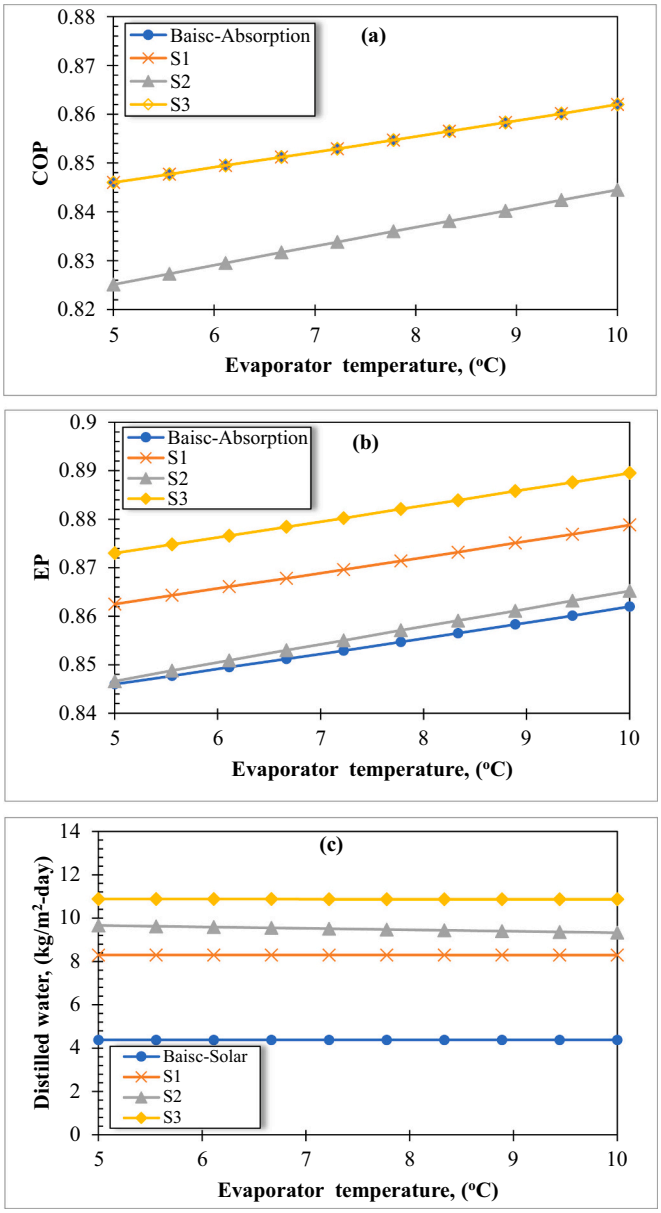


**Fig. 13.** Effect of the evaporation temperature on (a) COP, (b) EP, and (c) distilled water of the proposed systems. Note: In (c), the amount of the distilled water of the basic solar system does not change with the variation of the evaporator temperature and plotted here for comparison purposes.

reduction of the heat supplied to the generator is another way to control the operation of the absorption system at partial load.

Fig. 13(a) shows that the evaporator temperature increase from 5 to 10 °C improves the COP by 2% in all configurations. Also, the COP and EP of S2 are lower than of the other configurations except the basic one (Fig. 13(b)). Moreover, the EP of S3 is higher than of S1 and the basic absorption system. Furthermore, the variation of the evaporator temperature reduces the still productivity, minimally (Fig. 13(c)) in S1 and S2 due to the decrease of the refrigerant and absorbent mass flow rates. From the previous sections, it could be noted that S2 has better performance than of the basic configuration. S3 has a better effect on the still productivity but slightly increases the required area of the ETCs. S1 improves the still productivity, reduces the condenser load, and has no effect on the COP of the basic system.

### 4.4. *Effect of solar radiation*

The solar radiation has a major effect on the required area of the evacuated tube collector for the absorption system as well as on the productivity of the still as shown in Fig. 14. As the solar radiation increases, the required area of the ETCs is reduced since the energy concentration per square meter is increased. Also, the efficiency of the ETCs increases too as shown in Fig. 14(a). The solar still productivity increases linearly with solar radiation. In the basic configuration of the solar still, the productivity increases from 2.5 kg/m$^2$-day to 9 kg/m$^2$-day as the solar radiation increases from 300 W/m$^2$ to 1000 W/m$^2$. The productivity of the still is further enhanced in the other configurations. Compared to the basic configuration, S1 and S3 improve the still productivity two and three times higher than the basic solar still, respectively (notice that the error in the productivity calculations is 3.33 as verified by the validation with the experimental measurements shown in

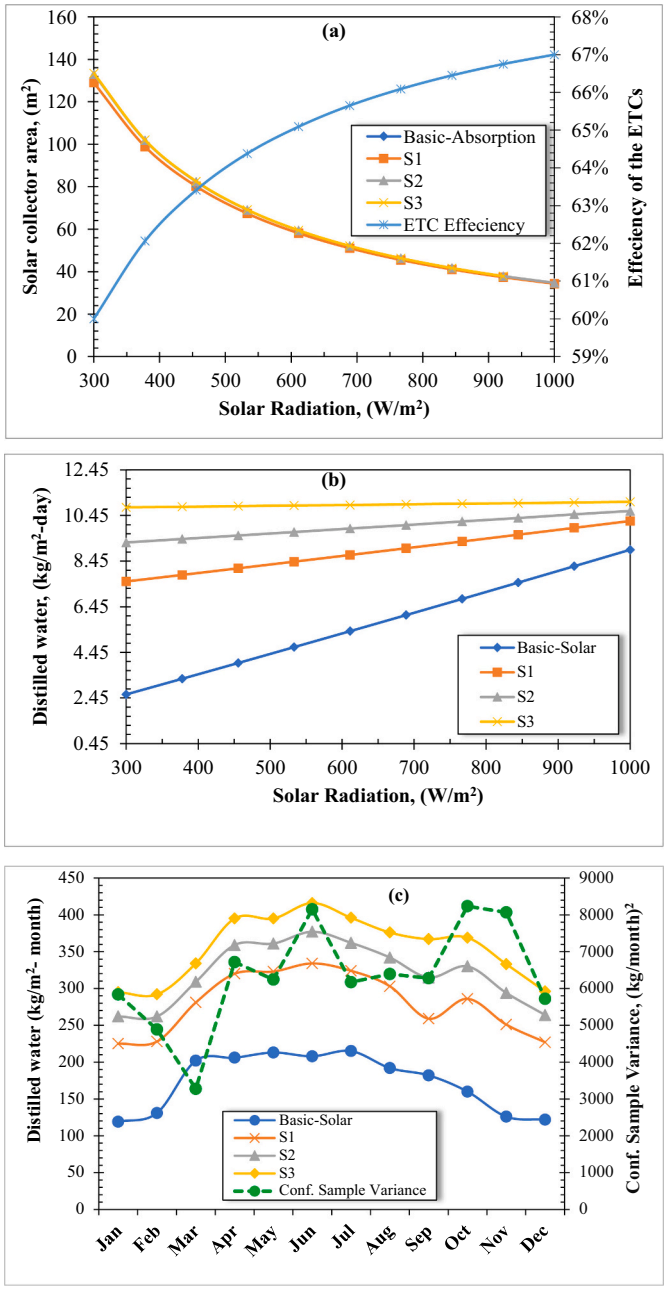


**Fig. 14.** (a) Relationship between the solar radiation and required area of the ETCs, (b) relationship between the solar radiation and solar still productivity, (c) estimated solar still productivity per month with the sample variance of the monthly productivity for the investigated configurations.

Table 5). As shown in Fig. 14(b), the productivity of all configurations are close to each other at high solar radiation. At the design conservative value of the solar radiation (500 W/m$^2$), the required area of the ETCs is 80 m$^2$ for a cooling capacity of 20 kW, and the still productivity is 4.5 kg/m$^2$-day for the basic configuration, 8.4 kg/m$^2$-day for S1, 9.5 kg/m$^2$-day for S2 and 10.9 kg/m$^2$-day for S3.

To estimate the actual productivity of the still more accurately, the average solar radiation on a horizontal surface and sunshine duration per month are presented in Table 6 and Fig. 14(c). The basic solar still yields 1868 kg/year. With heating and cooling enhancement, it yields 3361 kg/m$^2$-year in S1, 3837 kg/m$^2$-year in S2, and 4263 kg/m$^2$-year in S3. The difference between S1 and S2 is 476 kg/m$^2$-year and 902 kg/m$^2$-year between S1 and S3. It can be concluded that the integration of the absorption system and solar still system in S1 or S3 is more favorable than in S2.

To evaluate the variation of the monthly productivity of the basic still compared to the integrated solar still, the configuration sample variance (CSV) concept is used and defined as shown in Eq. (48) as:

$$CSV = \frac{1}{S-1}\sum_{i=1}^{S}\left(m_{\text{dist.conf.,i}} - \overline{m}_{\text{dist}}\right)^2 \quad (48)$$

where S is the number of configurations (M = 4), $m_{\text{dist. month, i}}$ is the productivity of each still per month, and $\overline{m}_{\text{dist.conf.}}$ is the average productivity of all configurations per month. Therefore, as the CSV increases, this means that the productivity of theses configurations significantly differ from the average productivity for all of them per each month. As, the CSV decreases, this means that the productivity of each still is close to the average productivity of all stills. On the other hand, to evaluate the variation of each still productivity over the year, the annual sample variance (ASV) is defined as:

$$ASV = \frac{1}{M-1}\sum_{i=1}^{M}\left(m_{\text{dist.month.,i}} - \overline{m}_{\text{dist,year}}\right)^2 \quad (49)$$

where $M$ is the number of months (M = 12), $m_{\text{dist. month., i}}$ is the monthly productivity for the specified configuration, and $\overline{m}_{\text{dist,year}}$ is the average productivity of the specifies still over the year. Higher values for the ASV means that the productivity of the still significantly differ from month to another while lower values means that the productivity of the still tends to be stable over the year.

Considering the CSV as shown in Table 6 (last column) and Fig. 14 (c), it can be noted that the CSV significantly affected by the average solar radiation and the sunshine duration per month. For the first three months (Jan, Feb, and Mar), the solar radiation and the sunshine duration increase to an average of 4.12 kWh/m$^2$/day and 253 h/month, respectively. Within this range, the productivity of the basic solar still increases with a rate higher than of the other configurations since the integrated solar stills (at low solar radiation) relay on the heat provided by the heating coil more than the heat obtained from the solar radiation. As the solar radiation increases, its effects on the integrated still become more significant and the CSV increases with a maximum variance obtained in Jun (which has the maximum solar radiation and the largest sunshine duration). This means that the productivity of the integrated solar stills is much higher than of the basic still during the months that have high solar radiation intensity and longer sunshine duration. Moreover, the monthly variances of the proposed configurations (last row in Table 6) are lower than of the basic configuration. This means that the still productivity of the proposed integrated stills is more stable over the year than the basic solar still.

### 4.5. Estimation of distilled water cost and EP comparison

To estimate the cost of the distilled water, let F be the fixed cost of the solar still structure (103 $ for the basic structure and 503 for solar still with heating and cooling coils). V is defined as the annual maintenance cost (which is taken as V = 0.3 F), N is the average lifetime of the solar still, $m_y$ is the productivity of the still per year (from Table 6), $C_N$ is the still cost (total for N years), $C_N = (F + V) * N$, $m_N$ is the still productivity after N year ($m_N = m_y * N$); so the cost of the distilled water is $C_L = C_N/m_N$. Assuming that the lifetime of the basic structure equals its payback period (as a reference), the payback period of the other configurations can be estimated as: $PBP = (C_N) / (C_{L,CSS} \times m_N)$. Applying this approach, the cost of the distilled water of the proposed configurations in this study is compared with the classic solar still CSS (reference), the proposed system by Madiouli et al. [56]., and with the integrated ejector-solar still system studied by Sleiti et al. [48] as shown in Table 7 and Fig. 15.

From Fig. 15(a), it can be noted that the cost of distilled water basic structure is the minimum. S3 cost is lower than S2 and S1 due to its higher productivity. However, this configuration increases the solar

**Table 6**
Data on average solar radiation, sunshine duration, and estimated monthly distilled water per 1 $m^2$ solar still in Doha, Qatar [57].

| $i$ | Month | Average solar radiation (horizontal surface) (kWh/$m^2$/day) | Sunshine duration (h/month) | $m_{dist,month,i}$ (kg/$m^2$-month) | | | | Conf. sample variance ((kg/$m^2$-month))$^2$ |
|---|---|---|---|---|---|---|---|---|
| | | | | Basic | S1 | S2 | S3 | |
| 1 | Jan | 3.32 | 244 | 119 | 225 | 262 | 295 | 5835 |
| 2 | Feb | 4.22 | 241 | 131 | 228 | 262 | 292 | 4887 |
| 3 | Mar | 4.82 | 274 | 202 | 281 | 309 | 334 | 3278 |
| 4 | Apr | 5.72 | 325 | 206 | 320 | 359 | 395 | 6714 |
| 5 | May | 6.89 | 325 | 213 | 323 | 361 | 395 | 6243 |
| 6 | Jun | 7.37 | 343 | 208 | 334 | 377 | 416 | 8150 |
| 7 | Jul | 6.98 | 326 | 215 | 324 | 362 | 396 | 6170 |
| 8 | Aug | 6.47 | 310 | 192 | 303 | 342 | 376 | 6390 |
| 9 | Sep | 5.76 | 305 | 182 | 259 | 315 | 367 | 14,008 |
| 10 | Oct | 4.8 | 305 | 160 | 286 | 330 | 369 | 8234 |
| 11 | Nov | 3.66 | 276 | 126 | 251 | 294 | 333 | 8066 |
| 12 | Dec | 3.12 | 245 | 122 | 227 | 264 | 296 | 5718 |
| Total still productivity per year $m_y$ (kg/$m^2$year) | | | | 1868 | 3361 | 3837 | 4263 | |
| Annual Sample Variance ((kg/$m^2$-month))$^2$ | | | | 2012 | 1699 | 1771 | 1942 | |

**Table 7**
Estimation of distilled water cost. Notice that the error in the productivity calculation is 3.33% as verified by the validation with the experimental measurements shown in Table 5.

| Design | F ($) | V ($/year) | N (years) | $m_y$ (kg/year) | $C_N$ ($) | $m_N$ (kg) | $C_L$ ($/kg) | Payback period (years) | EP | $C_{L,n}$ |
|---|---|---|---|---|---|---|---|---|---|---|
| Basic | 103 | 30.9 | 10 | 1872 | 412 | 18,724 | 0.022 | 3.28 | 0.47 | 0.047 |
| S1 | 503 | 150.9 | 10 | 3312 | 2012 | 33,123 | 0.061 | 5.46 | 0.83 | 0.073 |
| S2 | 503 | 150.9 | 10 | 3742 | 2012 | 37,430 | 0.054 | 4.83 | 0.76 | 0.071 |
| S3 | 503 | 150.9 | 10 | 4259 | 2012 | 42,592 | 0.047 | 7.05 | 0.84 | 0.056 |
| Ref. [48] | 503 | 150.9 | 10 | 5067 | 2012 | 50,674 | 0.040 | 5.9 | 0.6 | 0.067 |
| Ref. [56] | 850 | 255 | 10 | 1530 | 3400 | 15,300 | 0.220 | 33.01 | 0.078 | 2.821 |
| CSS | 103 | 30.9 | 10 | 612 | 412 | 6120 | 0.067 | 10 | 0.013 | 5.154 |

collector area of ETC which is not included in this estimation. Furthermore, the cost of the produced water in S1, S2, and S3 is about 2.77, 2.45, and 1.81 times higher than the cost of that produced by the basic solar still. To consider the gains due to energy savings for the integrated system and its effect on the distilled water cost, a normalized cost parameter is defined as $C_{L,n} = C_L/EP$ as shown in Table 7. It can be noted the normalized cost of S1, S2, and S3 is about 1.55, 1.51, and 1.20 times higher than the normalized cost of the basic configuration. However, the still productivity in proposed integrated systems S1, S2, and S3 is 1.76, 1.99, and 2.20 times higher than of the basic still. Moreover, the cost of the distilled water from the integration with the ejector system is lower than the present system. However, the absorption system configurations have higher energy performances than the studied systems by Sleiti et al. [48] and Madiouli et al. [56].

Fig. 15(b) compares the average cost of the product water and the maximum daily productivity of the basic and integrated configurations of the present study with those reported (by Kabeel et al. [58]) for various improved solar still configurations. The cost values in [58] were reported in 2010, so they have been transformed to the cost of 2021 by multiplying the original cost with the consumer price index (CPI = 1.20) as calculated by the CPI inflation calculator on the Website of the United State Department of Labor [59]. It can be noted that the costs of the present configurations (S1 to S3) is about 2–3 times higher than that of the basic and pyramid solar stills. However, they have similar or lower costs than that of the others types such as stills with solar collector and with sun tracking, Moreover, it can be noted that S3 has the highest productivity over the other configurations presented in Fig. 15(b). Therefore, taking into account the COP of the cooling system and the improvement of the solar still system, S1 and S3 of the present study are recommended while S2 should be avoided due to its poor performance relative to the other configurations.

### 4.6. Multi-objective optimization analyses

From the above discussion, it can be noted that there is a trade-off between the optimal conditions to obtain maximum COP and to obtain the highest amount of the distilled water. For instance, the maximum COP is achieved at low generator temperatures while the amount of the distilled water is maximum at high generator temperature. Therefore, single and multi-objective optimization analyses were performed to find an optimum decision for three objective functions including COP, EP, and $m_{distilled}$. The optimization methodology and results are discussed in the next subsection.

#### 4.6.1. Optimization methodology

The optimization process was conducted based on the genetic algorithm (GA) method which is considered as the most comprehensive, robust, and reliable methods. It intends to mimic the biological evaluation and works based on bio-inspired operators such as mutation, crossover, and selection [60]. Further, the GA method, which is a tool in the EES library, is not affected by the initial guess values like the other methods [61]. However, the bounds of the decision variable should be selected carefully since the initial population and subsequent stochastic selections are chosen from within these bounds. Fig. 16 outlines the steps of the optimization process using the GA method which are:

(1) Enter the bounds of the selected decision variables which are the generator temperature ($75 \le T_6\ ^\circ C \le 90$), absorber temperature ($30 \le T_3\ ^\circ C \le 30$), condenser temperature ($30 \le T_{11}\ ^\circ C \le 50$), evaporator temperature ($5 \le T_6\ ^\circ C \le 10$).
(2) Select one of the objective functions which are maximization the *COP* (*Max. COP*), maximization of the *EP* (*Max. EP*), maximization $m_{distilled}$ (*Max.* $m_{distilled}$), and maximization the multi-objective function (*Max. MOF*) which is defined as:

$$Max.MOF = w_1 \cdot COP + w_2 \cdot EP + w_3 \cdot \frac{m_{distilled}}{m_{distilled,basic}} \quad (50)$$

where $w_1$, $w_2$, and $w_3$ are weighting coefficients assigned for each objective function which are assumed to be ($w_1 = w_2 = w_3 = 1/3$) and

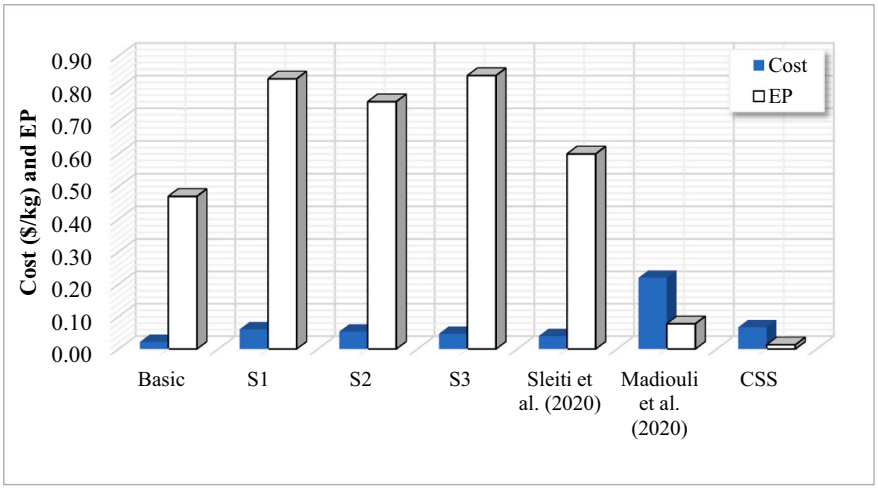


(a)

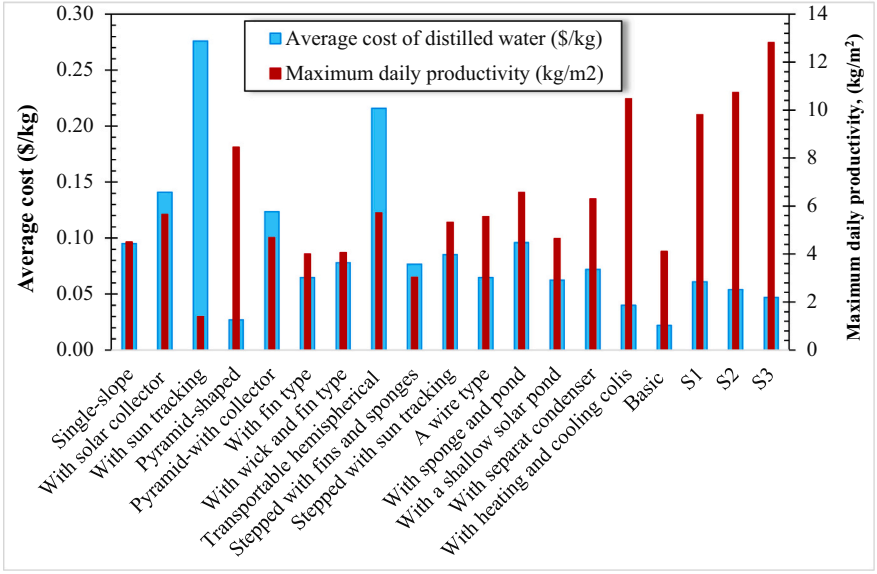


(b)

**Fig. 15.** (a) Comparison of the distilled water cost and energy performance (EP) of the present configurations with similar improved solar still systems, (b) comparison of the distilled water average costs and maximum daily productivities of various solar still types with the investigated configurations in the present study. Note: (b) was plotted based on data available in [58].

$m_{distilled,\ basic}$ is the amount of the distilled water produced by the basic solar still at the design point condition. $m_{distilled,\ basic}$ is inserted in the denominator of the third term of Eq. (50) to normalize it.

(3) Set the initial population by entering initial values for the most important variables of the GA method (number of individuals (16), number of generations (16), and the maximum maturation rate (20%)) which are responsible for identifying the optimum solution.

(4) Run the GA tool which works by generating initial random population of n individuals (fitness function) to evaluate the performance function (selection function). Then, a new population is created by repeating crossover, mutation and selection until the new population is completed. The new population is used for further run of the algorithm. If the termination criteria is satisfied, the process stops and returns the optimum solution in the current population. If GA fails to find the optimum, re-define the initial population parameters and run the GA until an optimized solution is obtained (see Fig. 16).

#### 4.6.2. Optimization results

Table 8 shows the optimized results of the objective functions and the corresponding decision variables for the basic and proposed configurations. It can be noted that the decision variables for the basic configuration are the same for the whole objective functions which are $T_6 = 75\ ^\circ C$, $T_3 = 30\ ^\circ C$, $T_{11} = 33.43\ ^\circ C$ and $T_1 = 10\ ^\circ C$ with COP of 0.88, EP of 0.88, and $m_{distilled}$ of 4.11 kg/day. However, for the proposed configurations, the decision variables differ based on the objective function. For example, lower generator, absorber, and condenser temperatures with high evaporator temperature are obtained if the objective function was *Max. COP* or *Max. EP*. The opposite is true if the objective function is *Max.* $m_{distilled}$. However, the results of the multi-objective function provides an optimal solution that keep the COP and the EP of the system at comparable values with those obtained by their single-objective functions with sufficient improvement in the productivity of the solar still as shown in Fig. 17.

Fig. 17 shows a comparison between the values of the objective parameters for the basic and the proposed configurations that were obtained by the MOF optimization. Compared to the results of the basic

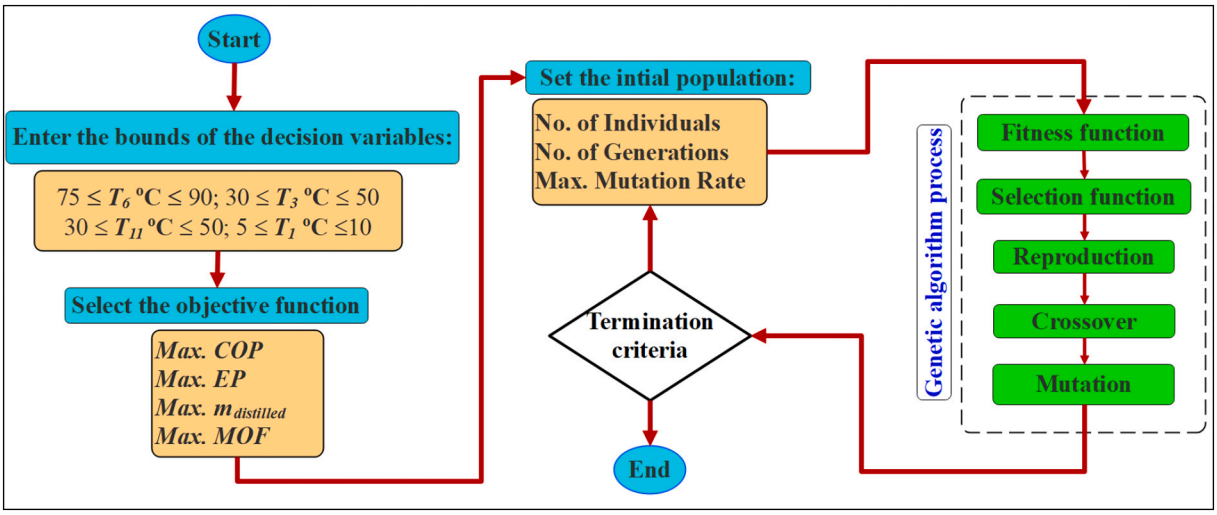


**Fig. 16.** Optimization procedures.

**Table 8**
Optimization results.

| Configuration | Optimization function | Decision variables | | | | Optimized results | | |
|---|---|---|---|---|---|---|---|---|
| | | $T_6$ [°C] | $T_3$ [°C] | $T_{11}$ [°C] | $T_1$ [°C] | COP | EP | $m_{distilled}$ [kg/day] |
| Basic | *Max. COP* | 75.00 | 30.00 | 33.43 | 10 | 0.88 | 0.88 | 4.11 |
| | *Max. EP* | 75.00 | 30.00 | 33.43 | 10.00 | 0.88 | 0.88 | 4.11 |
| | *Max. $m_{distilled}$* | 75.00 | 30.00 | 33.43 | 10.00 | 0.88 | 0.88 | 4.11 |
| | *Max. MOF* | 75.00 | 30.00 | 33.43 | 10.00 | 0.88 | 0.88 | 4.11 |
| S1 | *Max. COP* | 75.00 | 30.00 | 30.00 | 10.00 | 0.88 | 0.89 | 7.33 |
| | *Max. EP* | 75.00 | 30.00 | 31.37 | 9.90 | 0.88 | 0.89 | 7.33 |
| | *Max. $m_{distilled}$* | 94.99 | 31.71 | 49.50 | 5.15 | 0.82 | 0.85 | 9.92 |
| | *Max. MOF* | 94.92 | 30.00 | 30.00 | 8.98 | 0.86 | 0.88 | 9.80 |
| S2 | *Max. COP* | 75.00 | 30.00 | 30.00 | 10.00 | 0.86 | 0.87 | 8.07 |
| | *Max. EP* | 75.81 | 30.11 | 30.01 | 9.97 | 0.86 | 0.87 | 8.18 |
| | *Max. $m_{distilled}$* | 94.99 | 44.67 | 48.42 | 5.97 | 0.45 | 0.47 | 13.58 |
| | *Max. MOF* | 94.91 | 30.00 | 34.02 | 9.64 | 0.84 | 0.87 | 10.73 |
| S3 | *Max. COP* | 75.35 | 30.00 | 30.16 | 9.60 | 0.89 | 0.91 | 9.41 |
| | *Max. EP* | 75.03 | 30.00 | 30.00 | 9.98 | 0.89 | 0.91 | 9.34 |
| | *Max. $m_{distilled}$* | 93.88 | 41.38 | 45.25 | 5.40 | 0.76 | 0.80 | 13.46 |
| | *Max. MOF* | 91.13 | 30.16 | 30.02 | 8.77 | 0.86 | 0.90 | 12.81 |

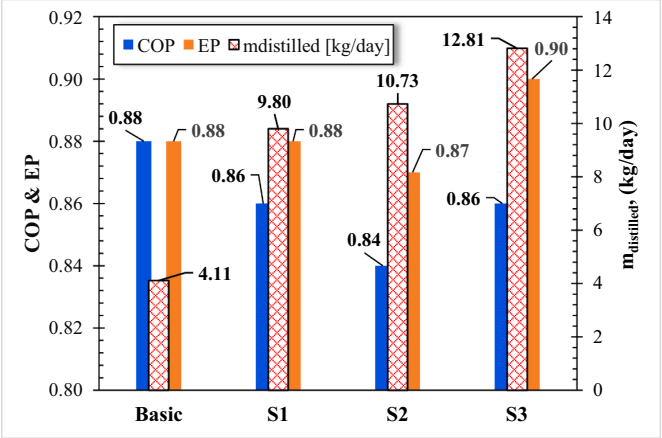


**Fig. 17.** Comparison of the optimized results obtained by the MOF.

configurations, it can be noted that the COP is reduced by 2%, in S1, 4.5% IN S2, and 2% in S3. The EP performance of S1 is the same as the basic absorption system (0.88) while the EP is reduced in S2 by 1% and improved in S3 by 2.27%. Moreover, the amount of the distilled water in S1, S2, and S3 is about 2.4, 2.6, and 3.1 times higher than the basic solar still, respectively. Form the multi-objective optimization results, it can be concluded that S3 has superior performance over the other configurations by providing the highest amount of distilled water and the maximum EP with comparable COP with the basic configuration with the following decision variables: $T_6 = 91.13$ °C, $T_3 = 30.16$ °C, $T_{11} = 30.02$ °C and $T_1 = 8.77$ °C.

## 5. Conclusions

A novel hybrid solar cooling and distillation system is designed, investigated and optimized. The system consists of a single-effect solar absorption system integrated with single-slope solar still. This integration aims at enhancing the solar still productivity by enhancing the evaporation and condensation processes. The heating and cooling processes in the coils are performed by the refrigerant of the absorption system. The cooling process is achieved by passing the refrigerant vapor through the cooling coil after it leaves the evaporator. The heating process is performed by recovering the waste heat from the flow streams leaving the generator in three configurations. S1 by recovering waste heat from the water vapor leaves the generator as it passes across the heating coil then proceeds to the condenser. S2 by passing the strong solution through the heating coil before the SHX. S3 by integrating the heating coil with the hot water leaves the generator to the evacuated tube collectors. The sensitivity of the proposed system to wide range of

operating parameters is analyzed and the cost of the distilled water is estimated and compared with similar improved solar still systems. The main conclusions are:

- The integration of the solar absorption cooling system with the solar still system boosted the water productivity of the still two folds in S1 and three folds in S3.
- S2 configuration negatively affected the COP of the absorption system, however, it improved still productivity to higher values than S1.
- The COP of S3 is comparable to that of S1, while the still productivity of S3 is the highest with a slight increase in the area of the ETCs.
- S1 has the advantage of enhancing solar still productivity and reducing the condenser cooling load without affecting the COP of the basic absorption system.
- Only S2 increases the still productivity with the increase of the absorber temperature.
- Within the range of the generator temperature, the EPs of S3, S2, and S1 are higher than their COP by 3.7%, 3.0%, and 2.2%, respectively.
- The increase of evaporator temperature from 5 to 10 °C improves the COP by 2% in all configurations.
- At solar radiation of 500 W/m$^2$, generator temperature of 90 °C, condenser temperature of 35 °C, evaporator temperature of 5 °C, and absorber temperature of 35 °C, a cooling capacity of 20 kW, and still productivity of 11 kg/m$^2$-day with COP of 0.85 are achieved in S3.
- The cost of the distilled water in S3 (0.047 $/kg) is lower than in S2 (0.054 $/kg) and S1 (0.061 $/kg).

## CRediT authorship contribution statement

**Ahmad K. Sleiti:** Conceptualization, Methodology, Investigation, Writing-Original draft, Review & editing, Funding acquisition, Supervision. **Wahib Al-Ammari:** Conceptualization, Writing-Original draft, Review & editing, Software, Visualization. **Mohammed Al-Khawajaa:** Conceptualization, Review & editing, Funding acquisition, Supervision.

## Declaration of competing interest

The authors declare that they have no known competing financial interests or personal relationships that could have appeared to influence the work reported in this paper.

*Acknowledgement*

The work presented in this publication was made possible by NPRP-S grant # [11S-1231-170155] from the Qatar National Research Fund (a member of Qatar Foundation). The findings herein reflect the work, and are solely the responsibility, of the authors.

## References

[1] M. Shublaq, A.K. Sleiti, Experimental analysis of water evaporation losses in cooling towers using filters, Appl. Therm. Eng. 175 (2020), 115418, https://doi.org/10.1016/j.applthermaleng.2020.115418.
[2] A.K. Sleiti, Tidal power technology review with potential applications in Gulf Stream, Renew, Sustain. Energy Rev. 69 (2017) 435–441, https://doi.org/10.1016/j.rser.2016.11.150.
[3] N. Abas, A. Kalair, N. Khan, Review of fossil fuels and future energy technologies, Futures. 69 (2015) 31–49, https://doi.org/10.1016/j.futures.2015.03.003.
[4] M. Höök, X. Tang, Depletion of fossil fuels and anthropogenic climate change-a review, Energy Policy 52 (2013) 797–809, https://doi.org/10.1016/j.enpol.2012.10.046.
[5] A.K. Sleiti, W.A. Al-Ammari, M. Al-Khawaja, Review of innovative approaches of thermo-mechanical refrigeration systems using low grade heat, Int. J. Energy Res. 44 (2020) 9808–9838, https://doi.org/10.1002/er.5556.
[6] A.K. Sleiti, M. Al-Khawaja, W.A. Al-Ammari, A combined thermo-mechanical refrigeration system with isobaric expander-compressor unit powered by low grade heat – design and analysis, Int. J. Refrig. 120 (2020) 39–49, https://doi.org/10.1016/j.ijrefrig.2020.08.017.
[7] A.K. Sleiti, W.A. Al-Ammari, M. Al- Khawaja, Analysis of novel regenerative thermo-mechanical refrigeration system integrated with isobaric engine, J. Energy Resour. Technol. 143 (2021) 1–10. doi:https://doi.org/10.1115/1.4049368.
[8] A.F. Altun, M. Kilic, Economic feasibility analysis with the parametric dynamic simulation of a single effect solar absorption cooling system for various climatic regions in Turkey, Renew, Energy. 152 (2020) 75–93, https://doi.org/10.1016/j.renene.2020.01.055.
[9] Z.Y. Xu, R.Z. Wang, Comparison of absorption refrigeration cycles for efficient air-cooled solar cooling, Sol, Energy. 172 (2018) 14–23, https://doi.org/10.1016/j.solener.2018.04.004.
[10] I. Sarbu, C. Sebarchievici, General review of solar-powered closed sorption refrigeration systems, Energy Convers, Manag. 105 (2015) 403–422, https://doi.org/10.1016/j.enconman.2015.07.084.
[11] Z.Y. Xu, R.Z. Wang, Comparison of CPC driven solar absorption cooling systems with single, double and variable effect absorption chillers, Sol, Energy. 158 (2017) 511–519, https://doi.org/10.1016/j.solener.2017.10.014.
[12] J.F. Chen, Y.J. Dai, R.Z. Wang, Experimental and analytical study on an air-cooled single effect LiBr-H2O absorption chiller driven by evacuated glass tube solar collector for cooling application in residential buildings, Sol, Energy. 151 (2017) 110–118, https://doi.org/10.1016/j.solener.2017.05.029.
[13] S. Manu, T.K. Chandrashekar, A simulation study on performance evaluation of single-stage LiBr–H2O vapor absorption heat pump for chip cooling, Int. J. Sustain. Built Environ. 5 (2016) 370–386, https://doi.org/10.1016/j.ijsbe.2016.08.002.
[14] A. Lubis, J. Jeong, K. Saito, N. Giannetti, H. Yabase, M. Idrus Alhamid, Nasruddin, Solar-assisted single-double-effect absorption chiller for use in Asian tropical climates, Renew, Energy. 99 (2016) 825–835, https://doi.org/10.1016/j.renene.2016.07.055.
[15] G. Grossman, Solar-powered systems for cooling, dehumidification and air-conditioning, Sol, Energy. 72 (2002) 53–62, https://doi.org/10.1016/S0038-092X(01)00090-1.
[16] D.S. Kim, C.A. Infante Ferreira, Solar refrigeration options - a state-of-the-art review, Int. J. Refrig. 31 (2008) 3–15, https://doi.org/10.1016/j.ijrefrig.2007.07.011.
[17] R. Nikbakhti, X. Wang, A.K. Hussein, A. Iranmanesh, Absorption cooling systems – review of various techniques for energy performance enhancement, Alexandria Eng. J. 59 (2020) 707–738, https://doi.org/10.1016/j.aej.2020.01.036.
[18] T. Rajaseenivasan, K. Kalidasa Murugavel, Theoretical and experimental investigation on double basin double slope solar still, Desalination. 319 (2013) 25–32, https://doi.org/10.1016/j.desal.2013.03.029.
[19] L. Sahota, G.N. Tiwari, Effect of Al2O3 nanoparticles on the performance of passive double slope solar still, Sol, Energy. 130 (2016) 260–272, https://doi.org/10.1016/j.solener.2016.02.018.
[20] H. Panchal, K.K. Sadasivuni, M. Israr, N. Thakar, Various techniques to enhance distillate output of tubular solar still: a review, Groundw, Sustain. Dev. 9 (2019), 100268, https://doi.org/10.1016/j.gsd.2019.100268.
[21] A.E. Kabeel, S.W. Sharshir, G.B. Abdelaziz, M.A. Halim, A. Swidan, Improving performance of tubular solar still by controlling the water depth and cover cooling, J. Clean. Prod. 233 (2019) 848–856, https://doi.org/10.1016/j.jclepro.2019.06.104.
[22] N. Rahbar, A. Asadi, E. Fotouhi-Bafghi, Performance evaluation of two solar stills of different geometries: tubular versus triangular: experimental study, numerical simulation, and second law analysis, Desalination. 443 (2018) 44–55, https://doi.org/10.1016/j.desal.2018.05.015.
[23] S. Karroute, A. Chaker, Effect of spherical geometry on the heat and mass transfer in a solar still, EPJ Appl. Phys. 66 (2014), 30903, https://doi.org/10.1051/epjap/2014130535.
[24] K.H. Nayi, K.V. Modi, Pyramid solar still: a comprehensive review, Renew, Sustain. Energy Rev. 81 (2018) 136–148, https://doi.org/10.1016/j.rser.2017.07.004.
[25] K.V. Modi, K.H. Nayi, Efficacy of forced condensation and forced evaporation with thermal energy storage material on square pyramid solar still, Renew, Energy. 153 (2020) 1307–1319, https://doi.org/10.1016/j.renene.2020.02.095.
[26] A.F. Muftah, K. Sopian, M.A. Alghoul, Performance of basin type stepped solar still enhanced with superior design concepts, Desalination. 435 (2018) 198–209, https://doi.org/10.1016/j.desal.2017.07.017.
[27] R. Sathyamurthy, S.A. El-Agouz, P.K. Nagarajan, J. Subramani, T. Arunkumar, D. Mageshbabu, B. Madhu, R. Bharathwaaj, N. Prakash, A review of integrating solar collectors to solar still, Renew, Sustain. Energy Rev. 77 (2017) 1069–1097, https://doi.org/10.1016/j.rser.2016.11.223.
[28] H. Hassan, M.S. Yousef, M. Fathy, M.S. Ahmed, Assessment of parabolic trough solar collector assisted solar still at various saline water mediums via energy, exergy, exergoeconomic, and enviroeconomic approaches, Renew, Energy. 155 (2020) 604–616, https://doi.org/10.1016/j.renene.2020.03.126.
[29] O. Bait, M. Si-Ameur, Tubular solar-energy collector integration: performance enhancement of classical distillation unit, Energy. 141 (2017) 818–838, https://doi.org/10.1016/j.energy.2017.09.110.
[30] O. Bait, Exergy, environ–economic and economic analyses of a tubular solar water heater assisted solar still, J. Clean. Prod. 212 (2019) 630–646, https://doi.org/10.1016/j.jclepro.2018.12.015.
[31] A.E. Kabeel, M.M. Khairat Dawood, K. Ramzy, T. Nabil, B. Elnaghi, A. Elkassar, Enhancement of single solar still integrated with solar dishes: an experimental approach, Energy Convers. Manag. 196 (2019) 165–174, https://doi.org/10.1016/j.enconman.2019.05.112.
[32] A.E. Kabeel, Y.A.F. El-Samadony, W.M. El-Maghlany, Comparative study on the solar still performance utilizing different PCM, Desalination. 432 (2018) 89–96, https://doi.org/10.1016/j.desal.2018.01.016.
[33] M. Jahanpanah, S.J. Sadatinejad, A. Kasaeian, M.H. Jahangir, H. Sarrafha, Experimental investigation of the effects of low-temperature phase change material on single-slope solar still, Desalination. 499 (2021), 114799, https://doi.org/10.1016/j.desal.2020.114799.

[34] M. Al-harahsheh, M. Abu-Arabi, H. Mousa, Z. Alzghoul, Solar desalination using solar still enhanced by external solar collector and PCM, Appl. Therm. Eng. 128 (2018) 1030–1040, https://doi.org/10.1016/j.applthermaleng.2017.09.073.
[35] M. Elashmawy, M. Alhadri, M.M.Z. Ahmed, Enhancing tubular solar still performance using novel PCM-tubes, Desalination. 500 (2021), 114880, https://doi.org/10.1016/j.desal.2020.114880.
[36] O. Bait, M. Si-Ameur, Enhanced heat and mass transfer in solar stills using nanofluids: a review, Sol, Energy. 170 (2018) 694–722, https://doi.org/10.1016/j.solener.2018.06.020.
[37] O. Bait, Direct and indirect solar–powered desalination processes loaded with nanoparticles: a review, Sustain, Energy Technol. Assessments. 37 (2020), 100597, https://doi.org/10.1016/j.seta.2019.100597.
[38] G. Sadeghi, S. Nazari, Retrofitting a thermoelectric-based solar still integrated with an evacuated tube collector utilizing an antibacterial-magnetic hybrid nanofluid, Desalination. 500 (2021), 114871, https://doi.org/10.1016/j.desal.2020.114871.
[39] E.F. El-Gazar, W.K. Zahra, H. Hassan, S.I. Rabia, Fractional modeling for enhancing the thermal performance of conventional solar still using hybrid nanofluid, energy and exergy analysis, Desalination. 503 (2021), 114847, https://doi.org/10.1016/j.desal.2020.114847.
[40] K. Elmaadawy, A.W. Kandeal, A. Khalil, M.R. Elkadeem, B. Liu, S.W. Sharshir, Performance improvement of double slope solar still via combinations of low cost materials integrated with glass cooling, Desalination. 500 (2021), 114856, https://doi.org/10.1016/j.desal.2020.114856.
[41] E.M.S. El-Said, S.M. Elshamy, A.E. Kabeel, Performance enhancement of a tubular solar still by utilizing wire mesh packing under harmonic motion, Desalination. 474 (2020), 114165, https://doi.org/10.1016/j.desal.2019.114165.
[42] Z.M. Omara, A.S. Abdullah, A.E. Kabeel, F.A. Essa, The cooling techniques of the solar stills' glass covers – a review, Renew, Sustain. Energy Rev. 78 (2017) 176–193, https://doi.org/10.1016/j.rser.2017.04.085.
[43] S. Nazari, H. Safarzadeh, M. Bahiraei, Performance improvement of a single slope solar still by employing thermoelectric cooling channel and copper oxide nanofluid: an experimental study, J. Clean. Prod. 208 (2019) 1041–1052, https://doi.org/10.1016/j.jclepro.2018.10.194.
[44] S. Shoeibi, N. Rahbar, A. Abedini Esfahlani, H. Kargarsharifabad, Application of simultaneous thermoelectric cooling and heating to improve the performance of a solar still: an experimental study and exergy analysis, Appl. Energy 263 (2020), 114581, https://doi.org/10.1016/j.apenergy.2020.114581.
[45] N. Rahbar, J.A. Esfahani, A. Asadi, An experimental investigation on productivity and performance of a new improved design portable asymmetrical solar still utilizing thermoelectric modules, Energy Convers. Manag. 118 (2016) 55–62, https://doi.org/10.1016/j.enconman.2016.03.052.
[46] S. Rastegar, H. Kargarsharifabad, N. Rahbar, M.B. Shafii, Distilled water production with combination of solar still and thermosyphon heat pipe heat exchanger coupled with indirect water bath heater – experimental study and thermoeconomic analysis, Appl. Therm. Eng. 176 (2020), https://doi.org/10.1016/j.applthermaleng.2020.115437.
[47] A.R. Abd Elbar, H. Hassan, An experimental work on the performance of new integration of photovoltaic panel with solar still in semi-arid climate conditions, Renew, Energy. 146 (2020) 1429–1443, https://doi.org/10.1016/j.renene.2019.07.069.
[48] A.K. Sleiti, W.A. Al-Ammaria, M. Al-Khawaja, A novel solar integrated distillation and cooling system - design and analysis, Sol, Energy. 206 (2020) 68–83, https://doi.org/10.1016/j.solener.2020.05.107.
[49] Y. A. Cengel, A. J. Ghajar, Heat and Mass Transfer, Fundamentals & Application, Fifth Edition in SI Units, 2015.
[50] S. Kumar, G.N. Tiwari, Estimation of convective mass transfer in solar distillation systems, Sol, Energy. 57 (1996) 459–464, https://doi.org/10.1016/S0038-092X(96)00122-3.
[51] K. Sampathkumar, T.V. Arjunan, P. Pitchandi, P. Senthilkumar, Active solar distillation-a detailed review, Renew, Sustain. Energy Rev. 14 (2010) 1503–1526, https://doi.org/10.1016/j.rser.2010.01.023.
[52] T. Jia, P. Dou, P. Chu, Y. Dai, Proposal and performance analysis of a novel solar-assisted resorption-subcooled compression hybrid heat pump system for space heating in cold climate condition, Renew, Energy. 150 (2020) 1136–1150, https://doi.org/10.1016/j.renene.2019.10.062.
[53] N.A.A. Qasem, S.M. Zubair, A.M. Abdallah, M.H. Elbassoussi, M.A. Ahmed, Novel and efficient integration of a humidification-dehumidification desalination system with an absorption refrigeration system, Appl. Energy 263 (2020), 114659, https://doi.org/10.1016/j.apenergy.2020.114659.
[54] M.A. Sharafeldin, G. Gróf, Efficiency of evacuated tube solar collector using WO3/Water nanofluid, Renew, Energy. 134 (2019) 453–460, https://doi.org/10.1016/j.renene.2018.11.010.
[55] R. Lizarte, M. Izquierdo, J.D. Marcos, E. Palacios, An innovative solar-driven directly air-cooled LiBr-H 2O absorption chiller prototype for residential use, Energy Build. 47 (2012) 1–11. doi:https://doi.org/10.1016/j.enbuild.2011.11.011.
[56] J. Madiouli, A. Lashin, I. Shigidi, I.A. Badruddin, A. Kessentini, Experimental study and evaluation of single slope solar still combined with flat plate collector, parabolic trough and packed bed, Sol, Energy. 196 (2020) 358–366, https://doi.org/10.1016/j.solener.2019.12.027.
[57] M.B. Elbeih, A.K. Sleiti, Analysis and optimization of concentrated solar power plant for application in arid climate, J. Energy Sci. Eng. 2021 (2021) 1–14, https://doi.org/10.1002/ese3.742.
[58] A.E. Kabeel, A.M. Hamed, S.A. El-Agouz, Cost analysis of different solar still configurations, Energy. 35 (2010) 2901–2908, https://doi.org/10.1016/j.energy.2010.03.021.
[59] United States Department of Labor, CPI inflation calculator, data tools. https://www.bls.gov/data/inflation_calculator.htm, 2021.
[60] A. Khadse, L. Blanchette, J. Kapat, S. Vasu, J. Hossain, A. Donazzolo, Optimization of supercritical CO2 Brayton cycle for simple cycle gas turbines exhaust heat recovery using genetic algorithm, J. Sol. Energy Eng. Trans. ASME. 140 (2018), https://doi.org/10.1115/1.4039446.
[61] S. Alharbi, M.L. Elsayed, L.C. Chow, Exergoeconomic analysis and optimization of an integrated system of supercritical CO2 Brayton cycle and multi-effect desalination, Energy. 197 (2020), 117225, https://doi.org/10.1016/j.energy.2020.117225.